Numerical Simulation of Ship-Floating Offshore Wind Turbine Collision Using the Coupled Eulerian-Lagrangian Approach

Auteur : Palaniswamy Chandrasekaran, Abhemanyu
Promoteur(s) : Rigo, Philippe
Faculté : Faculté des Sciences appliquées
Diplôme : Master : ingénieur civil mécanicien, à finalité spécialisée en "Advanced Ship Design"
Année académique : 2023-2024
URI/URL : http://hdl.handle.net/2268.2/22240

Universität Rostock

Traditio et Innovatio

LIÈGE université

With the support of the Erasmus+ Programme of the European Union

Numerical Simulation of Ship-Floating Offshore Wind Turbine Collision Using the Coupled Eulerian Lagrangian Approach

submitted on 30 July 2024

by

PALANISWAMY CHANDRASEKARAN Abhemanyu

37 Avenue du Champ de Manoeuvres | 44470 Carquefou | p.c.Abhemanyu@gmail.com

Student ID No.: 223202138

First Reviewer:

Prof. Patrick Kaeding

Chair of Ship Structures

University of Rostock

18051 Rostock

Germany

Second Reviewer:

Prof. Le Sourne Hervé

Chair of Mechanical Engineering

ICAM Engineering School

44470 Carquefou

France

EMship+ Advanced Design

Master Thesis

This page is intentionally left blank

Abstract

The offshore wind industry has experienced significant recent growth, and this trend is expected to continue. Collisions between ships and Floating Offshore Wind Turbines (FOWTs) pose a challenge to this industry. While several numerical and analytical tools have been developed to analyze the crashworthiness of FOWTs, there is insufficient experimental data to verify and validate these methods. This master's thesis aims to develop a numerical simulation framework using the Coupled Eulerian-Lagrangian (CEL) approach, potentially serving as a validation tool for other simplified methods.

The study begins by validating the fluid-structure interaction (FSI) forces obtained through the CEL method against results from Boundary Element Method (BEM) solvers, establishing the accuracy of the proposed approach. A detailed discussion on the proper modeling setup for CEL simulations is presented, addressing key considerations for realistic collision scenarios. Using the OC3-HYWIND spar as the reference turbine, the research compares results from lower-fidelity MCOL simulations with those from the higher-fidelity CEL approach.

This comparison highlights the strengths and limitations of each method in capturing the complex fluid-structure interaction physics during ship-FOWT collisions. The study critically examines the limitations of the CEL approach as a validation tool for ship-FOWT collisions. Areas where both approaches fall short are identified and potential avenues for future development and refinement are proposed.

Keywords : Floating Offshore Wind Turbines (FOWTs), Ship collision, Coupled Eulerian-Lagrangian (CEL), Validation, Fluid-structure interaction (FSI), Boundary Element Method (BEM), MCOL.

This page is intentionally left blank

Contents

List of Figures

List of Tables

List of Abbreviations

ALE Arbitray Lagrangian Eulerian

BEM Boundary Element Method

CAM Constant Added Mass

CEL Coupled Eulerian-Lagrangian

CLIS CONSTRAINED_LAGRANGE_IN_SOLID

COB Center of Buoyancy

COG Center of Gravity

DOF Degree of Freedom

FEA Finite Element Analysis

FFT Fast Fourier Transform

FOWT Floating Offshore Wind Turbine

FSI Fluid Structure Interaction

HPC High-Performance Computing

MPP Massively Parallel Processing

NLFEA Non-Linear Finite Element Analysis

NREL National Renewable Energy Laboratory

OSV Offshore Supply Vessel

RNA Rotor Nacelle Assembly

S-ALE Structured-ALE

SMP Shared Memory Parallel

TLP Tension Leg Platform

This page is intentionally left blank

Declaration of Authorship

I declare that this thesis and the work presented in it are my own and have been generated by me as the result of my own original research.

Where I have consulted the published work of others, this is always clearly attributed.

Where I have quoted from the work of others, the source is always given. With the exception of such quotations, this thesis is entirely my own work.

I have acknowledged all main sources of help.

Where the thesis is based on work done by myself jointly with others, I have made clear exactly what was done by others and what I have contributed myself.

This thesis contains no material that has been submitted previously, in whole or in part, for the award of any other academic degree or diploma.

I cede copyright of the thesis in favour of the University of ICAM and University of Rostock.

Date : 30 JULY 2024 **Signature :**

This page is intentionally left blank

1 INTRODUCTION

The global push for sustainable energy sources has led to a significant expansion of offshore wind farms in recent years. As the demand for clean energy continues to grow, Floating Offshore Wind Turbines (FOWT) have emerged as a promising solution for harnessing wind power in deeper waters. However, this rapid growth in offshore installations has also increased the risk of ship collisions with these structures, presenting a critical challenge for the offshore wind industry. The potential for ship-FOWT collisions is a serious concern that requires thorough investigation and mitigation strategies. Ship collisions with offshore structures constitute a complex area of study, encompassing aspects of naval architecture, structural engineering, probability theory, and maritime operations. These incidents can result in severe consequences, including structural damage, environmental pollution, and potential loss of life.
Several notable incidents in recent years have highlighted the risks associated with ship collisions in offshore environments:

1. On 24 April 2023, a cargo ship - PETRA L collided with a wind turbine at the Godewind 1 offshore wind farm in the North Sea (Buljan 2023). The collision resulted in massive damage on the ship's starboard side, resulting in a 5×3 meter hole in the hull and reported water ingress.

Figure 1: Damaged hull of Petra L after collision with a wind turbine; Source : Buljan (2023)

2. On 31 January 2022, the bulk carrier Julietta D collided with the tanker Pechora Star. After a hull breach and subsequent evacuation of the crew, the former ship drifted through

Hollandse Kust Zuid wind farm, colliding with one of the yet-to-be-constructed FOWT foundation (Buitendijk 2022).

Figure 2: Damaged wind turbine foundation after collision; Source : Buitendijk (2022)

3. On 23 April 2020, a 24-meter-long crew transfer vessel crashed into a wind turbine at the Borkum Riffgrund 1 offshore wind farm, in the German North Sea, resulting in injuries to several crew members (Safety4Sea 2020).

1.1 Physics of Ship Collisions

Ship collisions are characterized by complex physical interactions involving transfer of energy and momentum between the structures and also the surrounding environment. The initial kinetic energy of the striking ship is converted into kinetic energy and deformation energy of the structures involved. Additionally, a part of this initial energy is also transferred to the surrounding water. Kinetic energy of the collided structures and hydrodynamic effects of the surrounding water govern the external dynamics concerning the rigid body motions. The internal energy is characterized by the different deformation mechanisms and damage that may occur in the collided structures. The energy conservation equation for a ship colliding with a FOWT can be written as

$$K_0 = K_{ship} + K_{FOWT} + U_{ship} + U_{FOWT} + E_{Hydro} + E_{Other} \tag{1}$$

where, K_0 is the initial kinetic energy of the striking ship with the hydrodynamic added mass accounted for; K_{ship} & K_{FOWT} are the kinetic energies of the striking ship and the struck FOWT respectively; U_{ship} & U_{FOWT} are the internal energies of the striking ship and the struck FOWT respectively. E_{Hydro} is the contribution from work done by the hydrostatic and hydrodynamic forces (added mass and drag) on the collided structures. Energy transferred due to any other interactions such as sea waves, mooring line forces, wind effects are included in E_{Other}.

The structural damage is dependent on several factors such as the impact energy, shape and geometry of striking ship and the struck FOWT. The rigid body motions of the colliding bodies, directly influence the force-penetration curves and hence the deformation shape. The contribution from different deformation mechanisms are affected by the mass distribution and inertia properties of the ballast, tower and Rotor Nacelle Assembly (RNA). Environmental conditions such as wind and waves can also have an effect on the motion of the structures and consequently the damage (Bela et al. 2017).

1.2 Aim & Motivation

Traditional numerical methods are often based on several simplified assumptions and decoupled approaches. The ability of simplified approaches to accurately capture the complex interactions between ships, floating structures, and the surrounding fluid environment needs further investigation. By combining the strengths of Eulerian and Lagrangian formulations, the Coupled Eulerian-Lagrangian (CEL) approach seems a promising solution to model the complex Fluid Structure Interaction (FSI) effects during ship collisions. Nevertheless, the effectiveness and added value of using the CEL approach to model ship-FOWT collisions are still active areas of research..

This master's thesis aims to develop and implement a numerical simulation framework using the CEL approach to model ship-FOWT collisions. The research will focus on:

1. Developing a CEL model using the Arbitray Lagrangian Eulerian (ALE) formulation in LS-DYNA, that could accurately represent the FSI during collision events and serve as a benchmark for comparison with other methods.
2. Validating the FSI model in LS-DYNA ALE against other numerical approaches.
3. Comparing the results of a collision scenario using the CEL approach and a and a lower fidelity approach based on MCOL subroutine in LS-DYNA.
4. Identifying the main drawbacks and potential for improvement in both methods.

In this thesis, the main research question addressed concerns with the method used to analyze the collision scenario, rather than structural crashworthiness & design of the FOWT. The research focuses on the damage analysis on the FOWT. The effect of damage on the striking ship is not considered for the present work and the ship is systematically considered as non-deformable.

1.3 Organization of the thesis

The thesis is presented in 7 sections.

1. INTRODUCTION - The current section presents the context of the research and its alignment with the previous work done in the COLFOWT project.

2. LITERATURE REVIEW - A brief description of existing research work on ship collisions and use of ALE method in LS-DYNA is presented in this section. It is followed by a short summary describing the research gaps that are to be addressed in the current thesis.

3. THEORETICAL FOUNDATION - Two different approaches - LS-DYNA/MCOL & LS-DYNA/ALE used to simulate ship collisions are compared in this study. This section presents a short description of the theory behind the MCOL subroutine & ALE and penalty coupling approach in LS-DYNA.

4. MODELLING - A detailed description of modelling methods used for the simulations are presented in this section. The section describes modelling of the fluid domain needed for the CEL simulations, followed by the finite element model description of the wind turbine used for the study. It is followed by an explanation of the FSI setup.

5. VALIDATION OF FLUID STRUCTURE INTERACTION - The section explains the need to correctly set the FSI coupling parameters. The procedure adapted to validate the FSI model is explained in detail. It is followed by an explanation to the possible reasons for errors in FSI.

6. COLLISION EVENT SIMULATIONS - The complete simulation setups for the collision of a ship with the SPAR type FOWT is presented in this section. The description of the simulation setup is followed by a comparison of results obtained between MCOL and CEL simulations.

7. CONCLUSION - The final chapter of this thesis delves into the observations made using the two different approaches. The limitations of CEL approach and its inadequacy to serve as a validation tool to analyze ship-FOWT collisions is presented in detail. The possibilities for improvement in both methods (LS-DYNA/ALE & LS-DYNA/MCOL) are discussed as a scope for future work.

2 LITERATURE REVIEW

Crash worthiness of offshore structures has been a topic of research interest in the offshore sector. Several researchers have studied ship collisions against offshore structures (Yu and Amdahl (2018), Storheim and Amdahl (2014), Petersen and Pedersen (1981)). Different numerical and analytical methods were used to study ship collisions against offshore structures. Such studies help in understanding the collision mechanisms and improving the design of offshore structures. For the current thesis work, the focus on existing literature is limited to the CEL approach.

2.1 Simulations using LS-DYNA ALE

The ALE method has been widely used to simulate physical interactions of different natures. Only a few studies relating to fluid-structure interaction, but not involving ship collisions are discussed here.

Structures being subjected to slamming loads is a common scenario considered for design of ships and offshore structures. The ALE formulation in LS-DYNA was used by Yu et al. (2019) to numerically model the hydro-plastic slamming response of beams and stiffened panels. The numerical simulations were validated against experimental results obtained from drop tests of a rigid wedge and an elastic plate. The vertical force on the wedge during water entry is coherent with the experimental results. For the elastic plate dropped into water, the pressure and deflection are predicted with a reasonably good accuracy. But, the rigid body motion of the plate obtained from ALE simulation shows a phase difference with respect to the experimentally observed curves. Negative pressures leading to cavitation and ventilation phenomenon are not captured using the ALE simulation.

Stenius and Ros'en (2007) used the ALE method in LS-DYNA to model the hydrodynamic loads for hull-water impact. The idealized hull-water impact scenarios compared well with theoretical and experimental results. It was concluded that the stability of solution is highly dependent on the mesh density/contact-stiffness relation. It was also observed that a higher mesh density is necessary to accurately capture the peak pressure response, particularly for higher pressure gradients.

Meicke (2011) used the ALE method in LS-DYNA to model the fluid-structure interaction of a wave energy converter. The thesis work includes a clear description of modelling using the ALE method and the parameters to be tuned. Aspects related to the numerical stability of the ALE solution has been presented. Some useful modelling practices in regard to the meshing and setting of coupling parameters have also been discussed.

2.2 Ship Collision Studies using LS-DYNA ALE

Gagnon and Wang (2012), performed numerical simulation of a collision between a tanker and a bergy bit (a large piece of freshwater ice that has broken off from a glacier or an ice shelf). The hydrodynamic effects of the surrounding water are explicitly modelled using the ALE formulation. A parametric study was performed to determine the fluid element size to achieve reasonable accuracy of results. A fluid element size of 2m was chosen. Approximately 26 seconds of ship travel (~96m) was necessary to produce a stable bow wave. The sway motion of the bergy bit due to the bow wave is used as an index to validate the fluid-structure interaction. This strategy has been used by Gagnon and Derradji-Aouat (2006) to compare the results obtained from LS-DYNA ALE simulations to the experimental data obtained from tank test. In the latter study, only the front half of the icebreaker ship was used. The ship was allowed to travel a length of 35m for the formation of a stable bow wave.

The work by Song et al. (2016), compares the FSI method and the Constant Added Mass (CAM) method for simulating ice-structure collisions. The collision between a floating block and a mass of ice is simulated by both methods in LS-DYNA. The FSI in LS-DYNA has been validated by comparing the added mass coefficients of a spherical body and rectangular block to the results obtained from the potential flow solver WADAM. The numerical simulations of ice-structure collisions were also validated against experimental results. The accelerations of the floating block obtained from FSI simulations were in close agreement with the experimental results during the initial stage of response (22 milliseconds). The study concludes that the FSI method could provide more accurate results with higher computation costs. But, since the computational time required by the FSI method is one order of magnitude higher than CAM method, the authors suggest that the use of a carefully calibrated CAM model is desirable.

Ye et al. (2023), used the ALE method to simulate oblique ship-bridge collisions. The fluid structure interaction was verified using the same method as Song et al. (2016). The similar procedure has been repeated for the ship and the added mass coefficients are compared to results obtained from the potential flow solver WADAM. The effect of including ambient boundaries to allow for inflow/outflow has also been studied. The results between CAM method and FSI method are compared. Their study concludes that the CAM method maybe suitable for head-on collision scenarios, whereas for oblique collisions the impact duration and impulse are underestimated by the CAM method compared to FSI method.

The FSI of ship-ship collision was studied using LS-DYNA ALE by Song et al. (2017). The optimum mesh size was determined by applying a sway force to the rigid ship and checking the convergence of the sway displacement. A fluid mesh size of 1m was determined to be appropriate. The results of penetration and loss of initial kinetic energy were discussed. With the FSI method, a part of the initial kinetic energy is dissipated by the surrounding water. For a moving struck ship, the results of contact forces obtained from the FSI simulations were significantly different from the CAM simulations. But, for a stationary struck ship, both FSI and CAM methods predicted the energy dissipation in good agreement with each other and analytical formulations. The added mass coefficient of the ship varied with time for the FSI simulation, whereas in the CAM approach it is assumed constant. The study also shows that FSI simulations in LS-DYNA using the ALE approach is very time-consuming. The CPU time for ALE approach is one order of magnitude higher than the CAM approach.

Guo et al. (2022) studied the collision of a ship with a Tension Leg Platform (TLP) wind turbine using LS-DYNA ALE. The hydrodynamic effects of surrounding water for the striking ship was modelled using the CAM method. For the TLP, the ALE formulation was used. Unlike other studies on ship collisions, the authors used a Gruneisen equation of state to model the fluids (air & water). The research article shows that internal energy accounts for more than 80% of the total energy in the system. Throughout the collision process, the kinetic and internal energies transformed into each other. The kinematics of the striking ship and TLP and the contact forces are presented. The authors recommend the use of ALE method to analyze hydrodynamic effects during ship-FOWT collisions.

The thesis work on ship-ice collisions by Zong (2012), presents a detailed study on modelling FSI using the ALE formulation in LS-DYNA. Modelling gravity loads & hydrostatics and obtaining the added mass and damping coefficients for the ship and ice block are discussed in detail. Most of the simulations were performed on a High-Performance Computing (HPC) cluster using the LS-DYNA Massively Parallel Processing (MPP) version. Some difficulties associated with modelling FSI using ALE are described. The study states that the penalty coupling formulation is sensitive to the mesh geometry and size. A significant amount of modelling effort was required to set up the correct penalty coupling between the fluid and structure to achieve reasonable results. The study shows that the use of ALE formulation can be very time-consuming even with HPC clusters. An alternative method to include the added mass, hydrostatic restoring forces and damping terms, as user defined functions has been proposed by the author.

A study using both MCOL & S-ALE to investigate an equivalent added mass coefficient of the struck ship in sway motion during ship-ship collisions, is reported in ClassNK (2023). The sway velocity results obtained by both MCOL and S-ALE were identical. The energy absorbed by the struck ship at end of collision, had only 3 % difference between MCOL and S-ALE.

2.3 Summary

The ALE method in LS-DYNA has been used to simulate FSI problems of different types. The ALE method is effective for short duration FSI problems such as slamming, aircraft ditching etc. In case of ship collisions, there are several contradicting opinions on the use of ALE method. Some studies suggest the use of ALE method to analyze FSI of ship collisions. But, in most studies the nature of FSI forces and resulting rigid body kinematics have not been validated or only been partially validated. The added advantage of using the ALE method over MCOL or CAM method is still unclear. In scenarios involving ship-ship collisions, the relative importance of hydrodynamic forces is higher than of hydrostatic forces. Hence, the nature of hydrostatic forces using the ALE method has not been emphasized in existing literature. For a collision scenario involving a SPAR floater, the effect of hydrostatics (pitch restoring moment) is equally important. Similarly, the results from existing literature show that the ALE approach is able to simulate a bow wave which could have an impact on the rigid body motions of both striking and struck structures. But, the ability of ALE to accurately represent a bow wave has not been validated or discussed.

The present thesis work is conducted with the aim of validating the nature of FSI forces predicted by an ALE simulation, and study the added advantages of using ALE in LS-DYNA.

3 THEORETICAL FOUNDATION

Different approaches can be used to analyze internal damage mechanics and the external rigid body dynamics of ship collisions. It was demonstrated by Echeverry Jaramillo et al. (2019) that a decoupled approach to separately analyze internal mechanics and external dynamics is not well suited for ship-FOWT collisions. A semi-coupled approach involves use of two different solvers sequentially, but the water surrounding the floating structure(s) is not explicitly discretized. The output from one solver is the input to the other solver and vice-versa (Vandegar 2023). In a fully coupled approach, both fluid and structure are modelled. The equations governing the structure and fluid are solved simultaneously in relation to each other.

3.1 Coupled Eulerian Lagrangian Method

3.1.1 Arbitrary Lagrangian Eulerian

The ALE method is a computational technique that combines the advantages of both Lagrangian and Eulerian methods to model the dynamics of deformable objects and fluid-structure interactions (Donea et al. 2004). This method is particularly useful in simulations involving complex geometries and large deformations. The ALE method integrates the strengths of both the Eulerian and Lagrangian approaches by allowing the mesh to move and deform independently of the material. The mesh can be adapted to follow the material motion (Lagrangian) or remain fixed (Eulerian), or it can move in an arbitrary manner to optimize the computational process (Olovsson 2006)

Each computational time step in LS-DYNA ALE method involves 2 phases.

1. **Lagrangian Phase:** The incremental motion of the material is computed. The material and mesh move identically in this phase.

2. **Eulerian Phase:** The mesh is moved independently of the material position. Material is transported between cells due to the relative motion between the mesh and material. Remapping algorithms are applied to maintain a regular mesh while preserving the material surface position determined in the Lagrangian phase. This is also referred to as the advection/remap phase.

The time integration loop for ALE formulation is shown in figure -3. First the lagrangian time derivatives are computed by LS-DYNA and the history variables (stress, strain, nodal forces

& kinematic quantities) are updated. This is followed by computation of the relative motion between the mesh and material during the advection phase. The previously computed history variables are updated again (Olovsson 2006). The advection phase induces a mass flux of the material through the mesh cells, which in turn influences the critical time-step. The critical time-step is calculated such that a material particle will not flow across more than half a mesh element in one time-step. Consequently, the total simulation time may increase due to the additional advection phase.

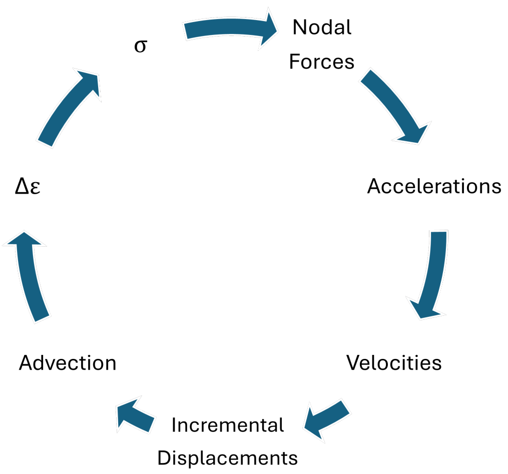

Figure 3: Time integration loop for ALE formulation; Source : Olovsson (2006)

Energy Balance in advection

Generally, conserving both kinetic energy and momentum simultaneously is not possible in the advection step (Eulerian phase). The advection algorithm is designed to conserve momentum with a loss in kinetic energy. As a result, a part of the total energy is lost in advection. To avoid this loss of energy, the advection method in `*CONTROL_ALE` keyword is set to **METH=3**. With this method the lost kinetic energy is converted and stored as the internal energy of the material (*LS-DYNA Keyword User's Manual* 2024a).

Compressibility and pressure equilibrium

In the ALE multi-material formulation, a mesh cell can be filled by two different materials with different compressibility. During the calculation, the entire mesh cell is treated as a single entity. This leads to materials with different compressibility in the same mesh cell, having the same strain rate. As a result, unrealistic behavior and dropping time-steps may occur. To avoid this the **PRIT** field must be set to 1 (Ian and Jim 2005). This allows for a pressure iteration algorithm to be activated, so that different materials within the same mesh cell can be exposed to different compressions.

3.1.2 Penalty Coupling

In LS-DYNA/ALE, a sequentially staggered coupling approach is used to solve the equations governing the fluid and structure. The mesh of the lagrangian solid structure and the Eulerian fluid overlap each other. The contact between the lagrangian and eulerian part is modelled like a spring force. The forces due to interaction is calculated as explained below (further details can be found in *LS-DYNA Theory Manual* (2024))

1. A number of coupling points are defined between the lagrangian and eulerian segments in contact. In case of a nodal penalty coupling, the coupling forces are directly applied on the lagrangian nodes.

2. The contact stiffness of an imaginary spring is calculated as

$$k_s = f_{si} \times \frac{K_i \cdot A_i}{max(\text{shell diagonal})} \tag{2}$$

, where f_{si} is a user-defined scale factor, K_i & A_i are the bulk modulus & face area of the element containing the segment - 'i' (a segment refers to a mesh face).

3. The penetration distance of the coupling points are measured.

4. Spring forces are applied to both the lagrangian and eulerian segments to push them away from each other.

The eulerian segment mentioned above refers to the material interface and not the mesh (refer figure-4)

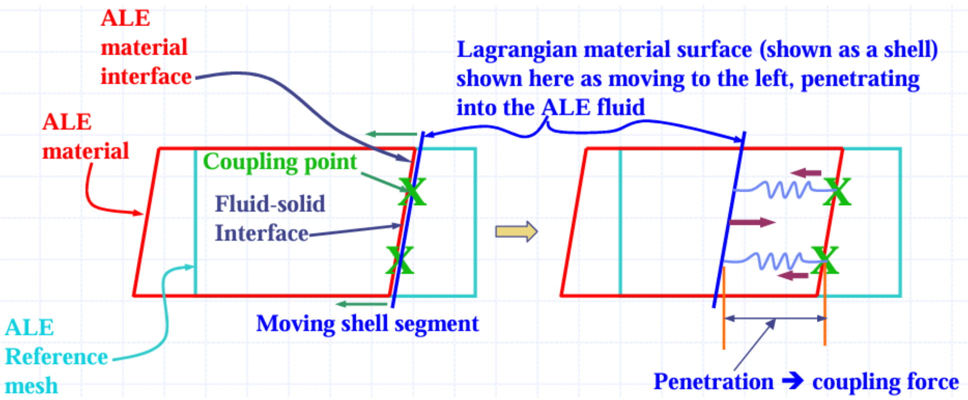

Figure 4: Coupling forces in ALE using penalty method; Source: Ian and Jim (2005)

A proper definition of the coupling points and stiffness is important to ensure accurate representation of the fluid-structure interaction. It must be noted that a highly stiff coupling could cause numerical instabilities and insufficient coupling stiffness can cause leakage problems. A set of options are also available to control leakage. The leakage control is an additional force similar to the penalty coupling force. This is applied when the primary coupling force is insufficient to prevent leakage.

3.1.3 Limitations of the ALE method

With the CEL approach, a penalty based coupling is used to model the fluid structure interactions. There are several limitations of modelling a fluid-structure interaction problem using penalty coupling in the ALE formulation (LS-DYNA Aerospace Working Group 2022). Some of them are listed below

1. The solver used is not a complete Navier-Stokes solver. Hence, it cannot account completely for the fluid viscosity effects such as boundary layer.

2. Turbulence models are not included in the solver, hence effects of vortex generation (e.g. drag effect) cannot be accurately modelled.

3. The compressible solver was developed for short duration simulations with high velocity gradients and is predominantly applicable for laminar flows.

4. The penalty coupling algorithm models fluid-structure interaction using imaginary springs that prevent a fluid element (Eulerian) from penetrating into a solid/shell element (Lagrangian). Hence the fluid-structure interaction force is always a function of the penetration, whereas in reality the fluid-structure interaction forces are proportional to accelerations (fluid inertial forces) and velocities (drag forces).

3.2 MCOL

MCOL is a rigid body dynamics solver, used to analyze ship collisions. The original MCOL (Mitsubishi collision) solver developed by Prof. Kitamura's team, was limited to small rotational movements. It was completely re-written by Le Sourne et al. (2001) to include effects of viscous damping & gyroscopic effects due to large rotations, for ship-submarine collisions. The striking and struck ships are considered as rigid bodies under action of collision forces and hydrodynamic forces (Le Sourne et al. 2003). The general form of equation for ship motion is written as

$$[M + M_{\infty}]\, \ddot{x} + G\dot{x} = F_W(x) + F_H(x) + F_V(x) + F_C \tag{3}$$

with $x = (x_{COG}, y_{COG}, z_{COG}, \phi, \theta, \psi)^T$ being the position of Center of Gravity (COG) of the ship, with respect to the earth fixed coordinate system. M is a 6×6 matrix representing the rigid body mass and inertia components of the ship. The hydrodynamic added mass and inertia of the ship are included in the M_∞ matrix. G is the gyroscopic matrix. F_W,F_H,F_V & F_C are the forces due to wave radiation damping, hydrostatic forces, viscous damping forces and contact forces respectively. Each force term on the right-hand side of equation -3 has three translational and three rotational components. The Non-Linear Finite Element Analysis (NLFEA) solver in LS-DYNA computes the contact force, which is input to MCOL to solve equation -3. The resulting kinematic quantities from MCOL are transferred to LS-DYNA and the loop continues. The coupling between LS-DYNA and MCOL is shown in figure - 5.

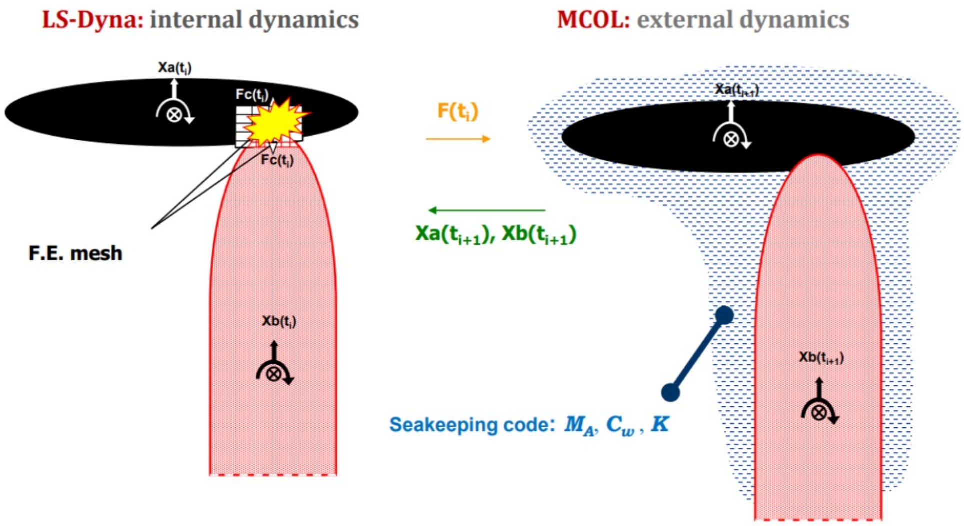

Figure 5: LS-DYNA/MCOL coupling ; Source: Le Sourne et al. (2001)

More details about how each of the forces in the right-hand side of equation -3 is computed, can be found in FERRY (2002a). The hydrostatic restoring matrix, added mass matrix (M_∞), viscous drag coefficient and wave damping matrices for different frequencies are user-defined inputs to MCOL (FERRY 2002b).

4 MODELLING

4.1 Fluid Domain Mesh

The fluid domain in LS-DYNA is modelled using a Structured-ALE (S-ALE) mesh composed of multi-material solid elements. At any instant of time, a solid element in the mesh may be filled by either air or water or a volume fraction of both. The newly developed S-ALE solver is intended to reduce errors in user inputs and enable easier set up of FSI simulations (Chen 2020). The nodes at the boundaries are given a free slip condition - the nodes can slip along the boundary faces, but cannot move in a direction normal to the boundary plane. Additionally, to model a semi-infinite fluid region, it is necessary to allow for pressure inflow/outflow at the boundaries of the ALE domain. To achieve this, one layer of elements in the boundaries are modelled as ambient elements (reservoir type). At each time step, the internal energies and volume fractions of these ambient elements are reset to their original values, as defined by their respective equations of state. These elements remain virtually unaffected during the simulation, hence modelling a semi-infinite fluid domain.

4.2 Fluid Material Models in LS DYNA

Several material models for air and water have been reported in literature. The commonly used material model for water is the **NULL** material with either one of the following equations of state - **Linear Polynomial**, **Murnaghan** & **Gruneisen**. A new material has also been developed to simulate incompressible flows in LS-DYNA (Aquelet and Souli 2013). But, as this material model does not support the initialization of hydrostatic pressures, it has not been used in this work.

For our simulations, seawater and air are modelled using the keyword `*MAT_NULL` in LS DYNA. The reference density ρ_0 and the coefficient of dynamic viscosity are defined using this keyword. Their physical behavior is modelled using a linear polynomial equation of state (*LS-DYNA Keyword User's Manual* 2024b).

$$P = C_0 + C_1\mu + C_2\mu^2 + C_3\mu^3 + (C_4 + C_5\mu + C_6\mu^2)E \tag{4}$$

$$
\begin{aligned}
P &= \text{pressure} \\
\mu &= \frac{\rho}{\rho_0} - 1 = \frac{1}{V/V_0} - 1 \\
\rho &= \text{current density} \\
\rho_0 &= \text{reference density} \\
V &= \text{current volume} \\
V_0 &= \text{reference volume} \\
E &= \text{internal energy per initial volume} \\
C_0, C_1, C_2, C_3, C_4, C_5, C_6 &= \text{user defined coefficients}
\end{aligned}
$$

It is important to properly specify the coefficients and the values of E_0 (initial internal energy per unit reference volume) and V_0 to achieve the correct initial pressures. In our simulations, the initial pressure is the same as atmospheric pressure, which is 101325 Pa and the initial relative volume $V_0 = 1$ (no compression or expansion).

Air

Air follows the gamma law equation of state with $\gamma = \frac{C_p}{C_v} = 1.4$ (C_p & C_v are specific heat coefficients of air at constant pressure and constant volume respectively). This can be modelled by setting

$$C_4 = C_5 = \gamma - 1 = 0.4$$

and setting all other coefficients (C_0, C_1, C_2, C_3, C_6) to zero. For the atmospheric pressure to be initialized correctly, the value of E_0, is calculated as follows

$$P = 101325 = (0.4 + 0.4\mu^2)E_0 \tag{5}$$

which yields the value $E_0 = 253312.5Pa$

Water

To model water using the linear polynomial equation of state, C_0 is set to the value of initial pressure and C_1 is set to the elastic bulk modulus of water. The bulk modulus maybe estimated as

$$C_1 = \rho_0 * c^2 \tag{6}$$

where $\rho_0 = 1025 kg/m^3$, is the reference density for seawater and 'c' is the speed of sound in seawater. The final value of the bulk modulus C_1 is taken as 2.25×10^9 Pa. The reference volume V_0 is taken as 1 and the initial internal energy per unit reference volume (E_0) is set to 0.

4.3 Gravity Load & Hydrostatic Pressure

To include the effect of buoyancy, it is necessary to correctly model gravity loads. In LS-DYNA the gravity force is modelled as an inertial force. A `*LOAD_BODY_Z` keyword is used to define the acceleration due to gravity with the vector pointing vertically upwards (positive z direction). This allows for the gravity to be included as an inertial force that acts downwards.

Modelling hydrostatic pressure in the fluid domain requires definition of additional keywords. Sudden initialization of gravity loads on the fluid at the start of simulation will cause unwanted pressure fluctuations in the fluid due to abrupt loading. Hence, gravity is scaled up gradually over a duration of 0.1 seconds. The hydrostatic pressure in the ambient boundaries is initialized using the keyword `*ALE_AMBIENT_HYDROSTATIC`. The same load curve used to ramp up gravity for both keywords - `*ALE_AMBIENT_HYDROSTATIC` & `*LOAD_BODY_Z`. This method automatically initializes the hydrostatic pressure inside the regular fluid domain and allows time for any Lagrangian objects in the domain to equilibrate to the correct position (*LS-DYNA Keyword User's Manual* 2024a).

With this approach the hydrostatic pressure in the ambient boundaries remains constant over time, whereas the pressure in the regular fluid domain still showed some fluctuations.

A method to include damping and eliminate pressure oscillations is described by Ye et al. (2023). The critical damping required for this is calculated by measuring the period of undamped pressure oscillations ($T_{undamped}$) as

$$c_{crit} = \frac{4\pi}{T_{undamped}} \tag{7}$$

Although this method can be effective in achieving a stable hydrostatic pressure in the main fluid domain, this could also include additional unnecessary damping forces in the FSI. Since the ALE advection step might already include some non-physical energy dissipation, this method of including damping is not preferred. Instead, the duration of gravity loading is increased. By increasing the duration of gravity load to 0.5 seconds, the pressure fluctuations were almost completely eliminated. The resulting pressure time-histories for different depths are shown for both cases in figure -6.

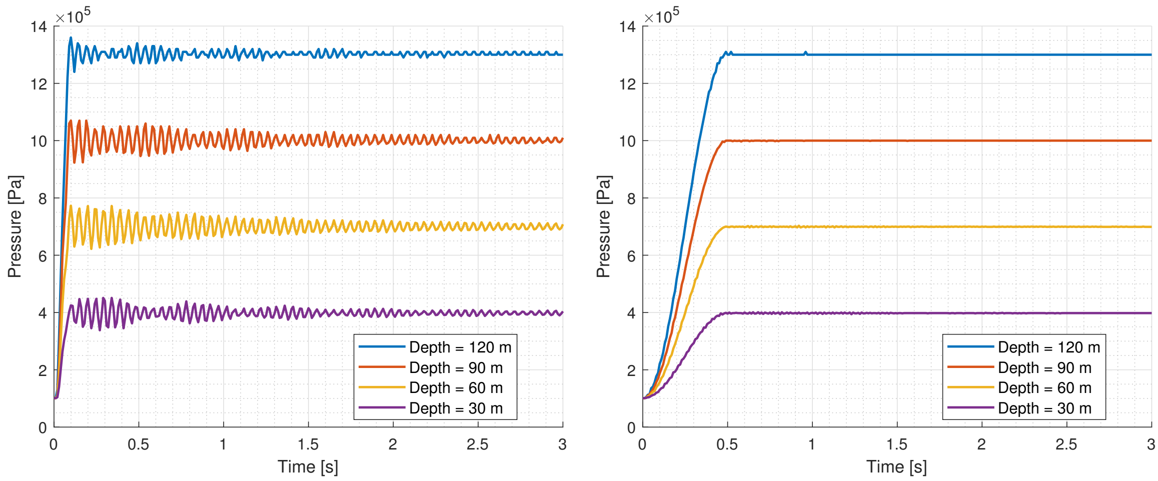

(a) Gravity loading over 0.1 seconds

(b) Gravity loading over 0.5 seconds

Figure 6: Pressure fluctuations observed at different depths

4.4 Finite Element Model of the FOWT

The numerical simulations are performed considering the 5MW National Renewable Energy Laboratory (NREL) reference wind turbine mounted on OC3 HYWIND spar platform. The dimensions, mass and inertia properties of the platform are listed in table-1. The SPAR and the tower are meshed using under-integrated Belytschko-Lin-Tsay shell elements. This element formulation is computationally very efficient and is commonly used to simulate collision scenarios. Five integration points are used through thickness of the shell element. The choice of element size is decided based on two factors:

1. A mesh sensitivity study was performed by Echeverry Jaramillo (2021) and a mesh size of 150 mm was recommended for regions where large deformations are expected.

2. A 1:1 mesh ratio between the lagrangian and eulerian parts is recommended for coupling using the ALE formulation. Hence, the coarse mesh region uses the same element size as the fluid mesh.

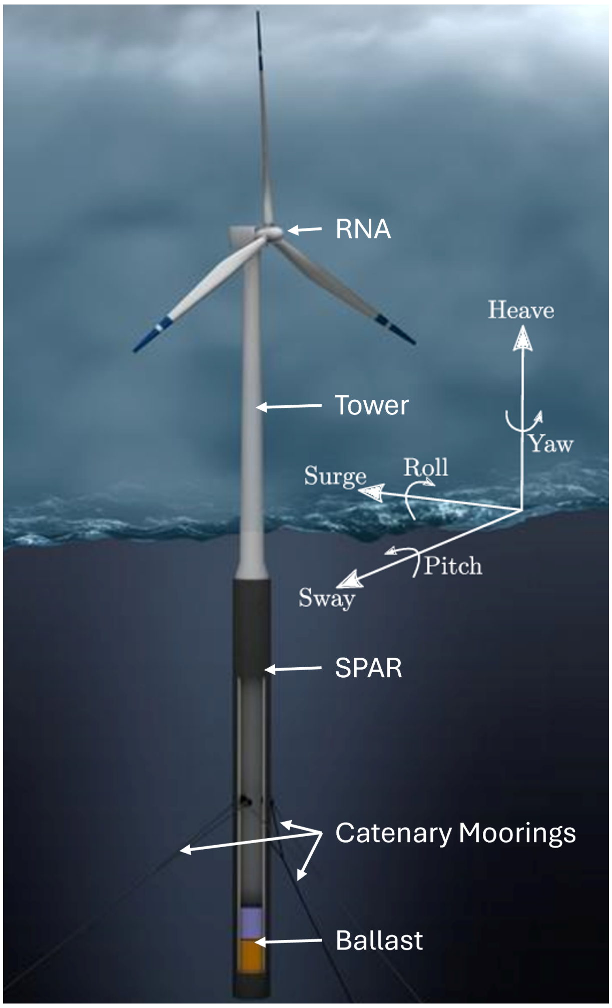

Figure 7: SPAR type FOWT ; Source: Chaaban and Fritzen (2014)

Table 1: Dimensions and mass properties of OC3 HYWIND SPAR with NREL 5MW wind turbine (Jason Jonkman 2010; J. Jonkman et al. 2009)

Depth to platform base below SWL	120 m
Water depth	320 m
Elevation to Platform Top (Tower Base) above SWL	10 m
Depth to top of taper below SWL	4 m
Depth to bottom of taper below SWL	12 m
Platform diameter above taper	6.5 m
Platform diameter below taper	9.4 m
Platform Mass including Ballast	7466.330 tons
Elevation to Tower Top (Yaw Bearing) above SWL	87.6 m
Platform COG below SWL	89.91 m
Total mass of tower	249.718 tons
Tower COG above SWL	43.4 m
Mass of Rotor Assembly (including blades)	110 tons
Rotor Assemby COG above SWL	90 m
Nacelle Mass	240 tons
Nacelle COG above SWL	89.35 m

Plastic-kinematic model available in LS-DYNA is used to model steel. The material properties for the tower and SPAR are summarized in table -2. For the FOWT tower, the density of steel is increased to account for paint, bolts, nuts and stiffening elements (Echeverry Jaramillo 2021; Jason Jonkman 2010). The strain rate effects are ignored in this study.

Table 2: Material properties for FE model of the FOWT

		FOWT Tower	**SPAR**
Density [kg/m^3]	ρ	8200	7800
Youngs Modulus [GPa]	E	210	210
Poisson's Ratio	ν	0.33	0.33
Yield Stress [MPa]	σ_y	255	255
Tangent Modulus [GPa]	E_{tan}	4	4
Failure Strain		0.2	-

To keep it simple, the finite element model used in this work does not include the stiffening elements for the turbine tower and the SPAR platform. However, in reality these structures are built with stiffening elements to resist crushing and buckling. In MCOL simulations, the effect of the surrounding fluid is handled separately and the resulting fluid-structure interaction loads are directly applied onto the COG of the SPAR. In CEL approach the surrounding water is explicitly modelled and the resulting FSI forces are not concentrated onto the COG of the structure anymore. Instead, they are distributed over the entire fluid-structure interface between the SPAR and surrounding water. For the initial validation studies presented in section-5.2, a uniform shell thickness of 8 cm was used to model the SPAR. But, it was observed that modelling the SPAR without stiffening led to crushing by external water pressure. In order to resolve this, the shell elements used for modelling the SPAR were made sufficiently thick to resist buckling due to external pressure. Increasing the thickness of the entire SPAR leads to a shift in the COG position and changes significantly the hydrostatic restoring behavior. The portion of the SPAR below the waterline is divided into sections of 12 m length. Each section is assumed to be an infinitely long isotropic unstiffened cylinder, and the minimum thickness required to resist buckling under hydrostatic pressure is calculated (Hilburger 2020).

$$p_{cr} = \frac{\gamma E}{4(1-\nu^2)} \left(\frac{t}{r}\right)^3 \tag{8}$$

p_{cr} = Critical buckling pressure	E = Young's modulus of the material
γ = Knockdown factor ≤ 1.0	ν = Poisson's ratio of the material
t = Cylinder wall thickness	r = Cylinder radius

The finite element mesh of the SPAR with the turbine tower is shown in figure-8. To keep the model axis-symmetric, one quarter of the mesh was modelled and mirrored about the vertical planes of symmetry. The SPAR below the waterline is modelled by 7 deformable parts. Each part is designed to be sufficiently thick to resist buckling under external hydrostatic pressure. The tower is modelled as 10 parts with the thickness varying from 27 mm at the base to 19 mm at the RNA end (Jason Jonkman 2010). The RNA is modelled as a rigid body, with its total mass and inertia tensor specified. Finally, a lumped mass is added to the bottom face of the SPAR. This allows to keep the COG and hydrostatic properties consistent with the actual reference model. The thickness and mass properties of the complete FE model of the FOWT used for CEL simulations, are shown in Appendix-A.

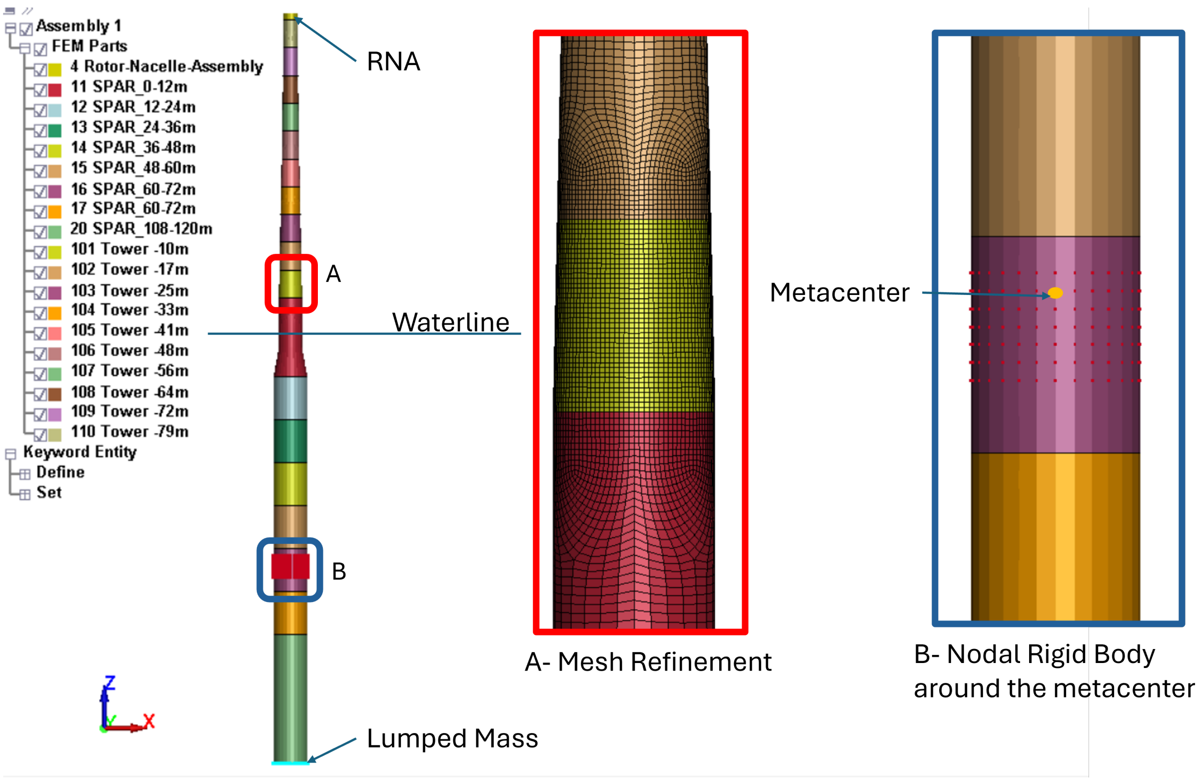

Figure 8: Finite Element Mesh of the SPAR and Tower

The MCOL subroutine in LS-DYNA allows for coupling only with rigid bodies. Hence, the section of the SPAR floater where the overall COG is located is modelled as a rigid body (using `*PART_INERTIA`) for MCOL simulations. With this change implemented, the mass of deformable bodies connected to the rigid body changed. As a result, the total mass of the finite element model is reduced. This difference in mass is calculated and added as additional lumped masses to the deformable parts, to keep the model consistent with the one used in CEL simulations.

4.5 Fluid-Structure Interaction

The new ALE_STRUCTURED_FSI keyword is used to set up the penalty coupling. Unlike the original CONSTRAINED_LAGRANGE_IN_SOLID (**CLIS**) keyword, which is conventionally used for setting FSI simulations in ALE, the new keyword reduces the number of inputs required. The penalty coupling algorithm is also improved for scalability in MPP. An improved algorithm always checks for leakage and corrects it. This method requires only the penalty coupling factor PFAC to be correctly set depending on the problem. The distribution of coupling points is automatically determined.

With this new keyword, the coupling force always acts only in the compression direction. This implies that the fluid cannot penetrate into the structure, but can freely move away from the structure. Hence, to set up a proper interaction model, at-least two of these same keywords are required. The first keyword prevents the water outside the lagrangian mesh to penetrate inside, and the second one prevents the air filled inside the lagrangian mesh from flowing out.

4.6 FSI Coupling Settings

Setting the coupling parameters specific to a problem is a tedious task. The penalty coupling is based on an ad-hoc approach and hence the correct settings can only be determined by trial and error. A systematic approach to finding the coupling settings was followed by positioning the finite element model of the SPAR in its floating equilibrium position. The SPAR is held fixed for the first 0.8 seconds hence allowing for a stable hydrostatic pressure to be formed in the fluid domain and then released. The coupling parameters are then varied as necessary to achieve a stable hydrostatic equilibrium and prevent leakage. The finite element model used to set the FSI coupling parameters is composed of shell elements, 1m in size without any refinement zones.

Using Default Settings

A first attempt is made by using the default values of PFAC=0.1 in LS-DYNA. The simulation was set up for a duration of 8 seconds. The time-step was continuously monitored over the run-time. After a simulation time of 0.26 seconds, the time-step decreased abruptly indicating possible errors in the simulation. On observing the pressure contours in the fluid domain, it was evident that the FSI coupling was too stiff and hence abruptly increased the fluid pressure close to the fluid-structure interface. To avoid this behavior, the values of PFAC must be reduced.

Estimating the value of PFAC required

The correct values of PFAC may lie in any range between 0 and 0.1. It is almost impossible to determine the correct values by trial and error. Hence, a more rational approach to identify the correct values of PFAC is followed based on the following assumptions.

1. The maximum pressure required is required at the bottom of the SPAR to avoid penetration of water into the structure. The maximum required pressure is assumed to be equal to $P_{atm} + \rho \cdot g \cdot H_{max}$, with P_{atm} and H_{max} being the atmospheric pressure and maximum expected depth at fluid structure interface respectively.

2. The penetration occurs in a direction normal to the shell element of the structure.

3. 4 coupling points are distributed over the shell element. (This is assumed based on the default values for NQUAD available from the **CLIS**)

4. FSI coupling forces act when the minimum volume fraction of the fluid penetrating into the structure is 0.5 (default values from **CLIS** keyword)

5. For coupling with air, the maximum pressure is always the atmospheric pressure (P_{atm}).

6. The S-ALE mesh is made of hexahedral elements of length l_e.

7. The size ratio for the structural shell elements and S-ALE hexahedral elements is 1:1.

The required value of PFAC is estimated as

$$P_{atm} + \rho \cdot g \cdot H_{max} = \frac{Coupling\ force}{Shell\ Area}$$

$$P_{atm} + \rho \cdot g \cdot H_{max} = \frac{n_{coupling\ points} \times Coupling\ Stiffness \times d_{penetration}}{Shell\ Area}$$

from equation-2,

$$P_{atm} + \rho \cdot g \cdot H_{max} = 4 \times \frac{1}{l_e \times l_e} \times \frac{PFAC \times K_i \cdot A_i}{max(Shell\ diagonal)} \times 0.5 \times l_e$$

$$P_{atm} + \rho \cdot g \cdot H_{max} = 4 \times \frac{1}{l_e \times l_e} \times \frac{PFAC \times K_i \times l_e^2}{\sqrt{2} \times l_e} \times 0.5 \times l_e$$

$$P_{atm} + \rho \cdot g \cdot H_{max} = \frac{4 \times PFAC \times K_i \times 0.5}{\sqrt{2}}$$

Assuming $P_{atm} + \rho \cdot g \cdot H_{max} = 1.36 \times 10^6$ Pa and the bulk modulus of steel $K_i = 175$ GPa, the estimated value of PFAC is 5.5×10^{-6} for coupling with water. Similarly, for coupling with air the value of PFAC is estimated as 4.1×10^{-7}. While validating the FSI forces (section -5.2), these parameters are observed to be very soft to prevent leakage. Hence, they are not used.

Using Coupling Pressure Curves

Using a load curve to explicitly provide coupling pressure as a function of the penetration distance is the most recommended method (LS-DYNA Aerospace Working Group 2022; Chen 2020). To start, the load curve is constructed as a straight line. The line starts at origin, ends at a point with abscissa as 0.1 times the minimum ALE element size and ordinate as the maximum coupling pressure. Initially the maximum coupling pressure for water is assumed as the maximum hydrostatic pressure. Similarly, for air, the maximum coupling pressure is assumed to be the atmospheric pressure. The coupling pressure curve is further improved by observing the fluid penetration and the pressure in the fluid at the location where fluid leaks through the structure. This method proved to be very time-consuming to construct a reasonably accurate coupling pressure curve. Furthermore, the method did not yield any significant improvement in the results for the added mass computed in section 5.2, compared to using a constant value for PFAC.

5 VALIDATION OF FLUID STRUCTURE INTERACTION

As discussed in section-3.1.3, the CEL approach poses some limitations with respect to modelling the physical behavior of water, and especially regarding the correct value of PFAC to be used for air-structure and water-structure couplings. This creates a need to verify and validate the fluid-structure interaction model for any particular application. For the simulation involving collision of an OSV with a SPAR turbine platform, the effects of hydrostatics and hydrodynamic added mass play an important role in the rigid body motions of the impacted SPAR platform. Hence, the fluid-structure interaction using a penalty based coupling is validated against analytical formulations for the hydrodynamic added mass.

Similarly, the effect of the bow wave generated by the OSV before impact is important and requires validation. This is done by comparing the height of the bow wave generated in LS-DYNA ALE simulation with the height obtained from a potential flow solver.

5.1 FSI Coupling

Setting correct coupling parameters is important for the CEL approach. The penalty coupling setting must be able to replicate the physics of fluid structure interaction as accurately as possible. Unlike other solution methods for FSI, the penalty coupling algorithm with ALE formulation allows for fluid to penetrate into the structure and then calculates the coupling forces. To ensure proper FSI in the simulation, it should be verified if the coupling setting is adequate to maintain a proper interface between the fluid and structure throughout the simulation. Errors in the fluid-structure interface could lead to "**Artificial Added Mass Effect**" and make the solution unstable. This effect is briefly explained in section-5.4. As observed from existing studies using the ALE formulation (Meicke 2011; Zong 2012), setting the correct penalty stiffness is a tedious task. Several iterations are needed to identify the correct penalty settings. The coupling settings used for simulations are not explicitly stated in studies involving ship collisions (ClassNK 2023; Guo et al. 2022; Song et al. 2017). The commonly used fluid mesh size in existing literature is in the range of 1 m-2 m. A fluid mesh size less than 500 mm has not been reported for a full scale simulation. Hence, to proceed with further validation a mesh size of 1m is chosen, by considering the total computational time.

The rigid body motion of the SPAR during collision is affected by the hydrostatic restoring forces and hydrodynamic added mass forces. Among the different DOFs, the important ones affecting the force-penetration curves are surge and pitch. The hydrostatic forces are linear and can be replicated as spring forces, whereas the nature of hydrodynamic forces are non-linear. Hence, accurate representation of the hydrodynamic added mass (in surge) using the CEL approach is given more importance in this study.

5.2 Hydrodynamic Added Mass

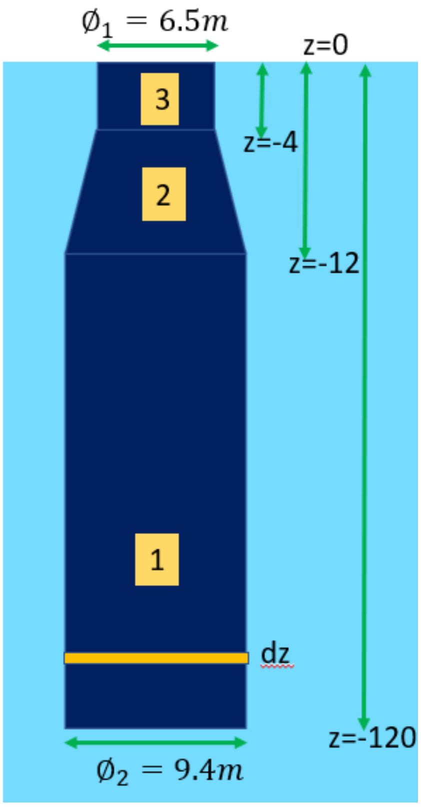

Figure 9: Geometry of Hywind Platform below waterline

In design of offshore structures, "**Strip Theory**" is widely used to compute the added mass of fixed and floating structures. For a circular cross-section of diameter "ϕ", the coefficient of added mass(C_A) is taken as 1 and the added mass per unit length (dM_{added}) is given by

$$dM_{added} = \rho \cdot C_A \cdot \frac{\pi}{4} \cdot \phi^2 \tag{9}$$

The analytical value of added mass for the OC3 HYWIND SPAR platform geometry shown in figure -9, is obtained by integrating along the submerged length as

$$A_{xx} = A_1 + A_2 + A_3$$

$$A_1 = \int_{-120}^{-12} \rho \cdot \frac{\pi}{4} \cdot C_A \cdot {\phi_2}^2 dz \qquad A_2 = \int_{-12}^{-4} \rho \cdot \frac{\pi}{4} \cdot C_A \cdot \phi^2 dz \qquad A_3 = \int_{-4}^{0} \rho \cdot \frac{\pi}{4} \cdot C_A \cdot {\phi_1}^2 dz$$

$$A_{xx} = 1025 \times 1 \times \frac{\pi}{4} \times \left(\int_{-120}^{-12} 9.4^2 dz + \int_{-12}^{-4} (9.4 - 0.3625z)^2 dz + \int_{-4}^{0} 6.5^2 dz \right)$$

$$A_{xx} = 8.2230 \times 10^6 \text{kg}$$

The added mass in surge is also compared with values obtained from the commercial hydrodynamics software package - ANSYS AQWA. The value of added mass at infinite frequency obtained from ANSYS AQWA is 7.859×10^6kg. AQWA uses the Boundary Element Method (BEM) and accounts for the diffraction and radiation effects at the free surface, whereas these effects are not accounted for in the analytical formulations using Strip Theory. Hence, a difference in added mass values is observed. The values obtained from ANSYS AQWA using BEM can be considered more reliable.

To compute the added mass obtained from LS DYNA ALE simulations, Song et al. (2016), applied a harmonic load to the floating structures and post processed the acceleration and velocities. In surge or sway direction, the equation of motion for the SPAR platform maybe written as

$$(M + M_a)\ddot{x} + C\dot{x} + Kx = F_x \tag{10}$$

$$\begin{aligned} M &= \text{Mass of rigid body} \\ M_a &= \text{Added Mass in surge direction} \\ C &= \text{Linearized damping coefficient} \\ K &= \text{Hydrostatic restoring coefficient} \\ F_x &= \text{Total external force in surge direction} \end{aligned}$$

The term Kx is zero as there is no hydrostatic restoring force acting in the surge or sway direction, when mooring system is not considered. When the velocity ($\dot{x}$) is zero, the only contribution is the inertial force, which is a sum of the rigid body inertia and the hydrodynamic added mass.

At the time instants where the velocity is zero, the added mass is calculated as

$$M_a = \frac{F_x}{\ddot{x}} - M \tag{11}$$

Finally the added mass values computed at different time instants where velocities become zero can be averaged.

To ensure that the time evolution of added mass forces are correctly represented, a different procedure to calculate the added mass is followed. The **Morison's Equation** (equation - 12) is used to calculate FSI forces due to oscillatory flows around a cylinder and has been experimentally validated (Morison et al. 1950). The force history of the SPAR is compared to the **Morison's Equation**. The added mass coefficients and drag coefficients are calculated by method of the least squares.

$$F_{ext} = (M + M_a) \cdot \ddot{x} + \frac{1}{2} \cdot \rho \cdot A_{proj} \cdot \dot{x}|\dot{x}| \tag{12}$$

When a prescribed sinusoidal load is applied to the floater in surge direction, the resulting acceleration of the rigid body is also sinusoidal. As a result, a constant of integration is added to the displacement and velocity. The constant term could lead to the SPAR moving very close to/out of the fluid boundaries. To avoid this, a harmonic displacement of $x = x_a sin(\omega t)$ is imposed on the SPAR platform. The resulting total external force and acceleration time history of the SPAR is extracted. A sampling frequency of 60 Hz is used. The high frequency oscillations which occur in the solution due to numerical integration methods and time marching schemes, are filtered out using a Butterworth filter with a low pass frequency of 6 Hz.

From results of initial simulations, it is observed that the correct choice of coupling stiffness (i.e. the PFAC value) depends on several factors. The fluid penetration at a time-step is used to calculate the required coupling forces, but these forces are applied to the interface only in the next time-step. As a result, the magnitude of time-step and the kinematic quantities of the rigid body motion have an influence on the coupling stiffness parameters. The time-step for the SPAR being modelled as a rigid body is roughly 10 times higher than for a deformable body. In the final collision event simulation, a part of the SPAR below the waterline will be modelled as a deformable body. So, a deformable finite element model is used for the validation tests as well. The finite element used for the validation test has no mesh refinement zone. This can significantly reduce the number of shell elements and decrease the total computational time.

Choice of oscillating frequency and velocities

It is necessary to choose the coupling stiffness that is suited for the rigid body motion of the SPAR during and after collision with the OSV. The velocity and acceleration time history of the SPAR are analyzed from MCOL simulation data available from Echeverry Jaramillo (2021). The maximum expected velocity for the SPAR in surge after the collision event is 2 m/s. A Fast

Fourier Transform (FFT) is used to obtain the frequencies dominating the rigid body motion oscillations. The frequencies below 1 Hz have the highest contribution to the rigid body motion of the SPAR in surge/sway direction.

Choice of PFAC

It was observed from several simulations that setting the default value of 0.1 for coupling the structure to the air caused advection errors and causes the simulation to crash. After several iterations of testing, it is observed that a PFAC value of 1×10^{-5} helps in sufficiently preventing leakage of air out of the SPAR, while also maintaining the numerical stability of the solution. This value of PFAC is used for all further simulations for coupling the structure with air.
To identify the correct parameters to couple the structure with water, a sensitivity analysis is performed by varying the PFAC values. The mesh size is fixed at 1 m and a 1:1 ratio is maintained between the lagrangian and S-ALE meshes. The value of PFAC is initially varied in a logarithmic scale. The SPAR is given a harmonic displacement $x = 0.3334sin(6t)$. A sensitivity analysis is performed for the value of PFAC and the coefficients are measured. The measured values for added mass and drag coefficients are shown in figure - 10. The quality of the regression fit is also analyzed by observing the mean square error and R-squared values. The trend in variation of added mass and drag coefficient with PFAC is observed. The measured values for added mass and drag coefficients are always overestimated compared to the values obtained from potential flow solution and theory (C_m = 0.969 & C_D = 0.6).

PFAC $< 1 \times 10^{-5}$ cause problems of leakage at the bottom section of the SPAR, while PFAC $> 5 \times 10^{-4}$ report unrealistically negative values of added mass. The observations are coherent with the theoretical understanding of the penalty factor. With decreasing PFAC, the coupling stiffness is insufficient to prevent leakage, while increasing PFAC values cause the penalty coupling to be over-stiff hence leading to oscillations of the fluid-structure coupling force. The resulting force history curves for varying PFAC values are shown in figure-11

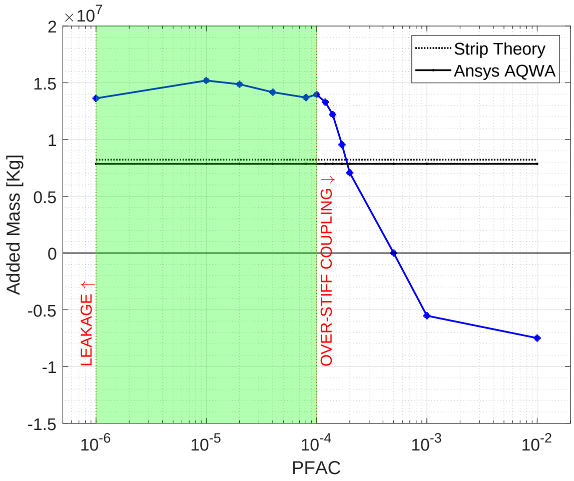

(a) Hydrodynamic Added Mass

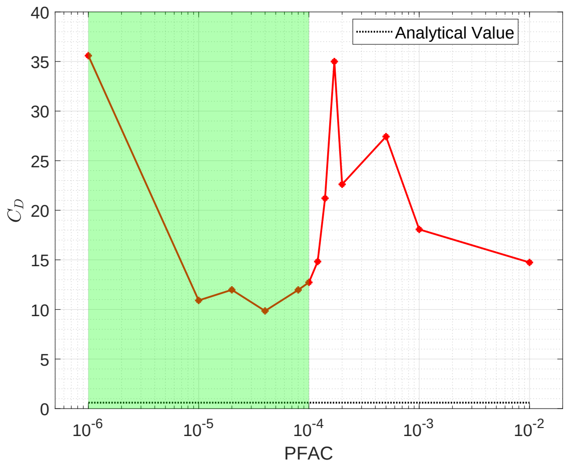

(b) Drag Coefficient - C_D

Figure 10: Variation of SPAR hydrodynamic properties with PFAC

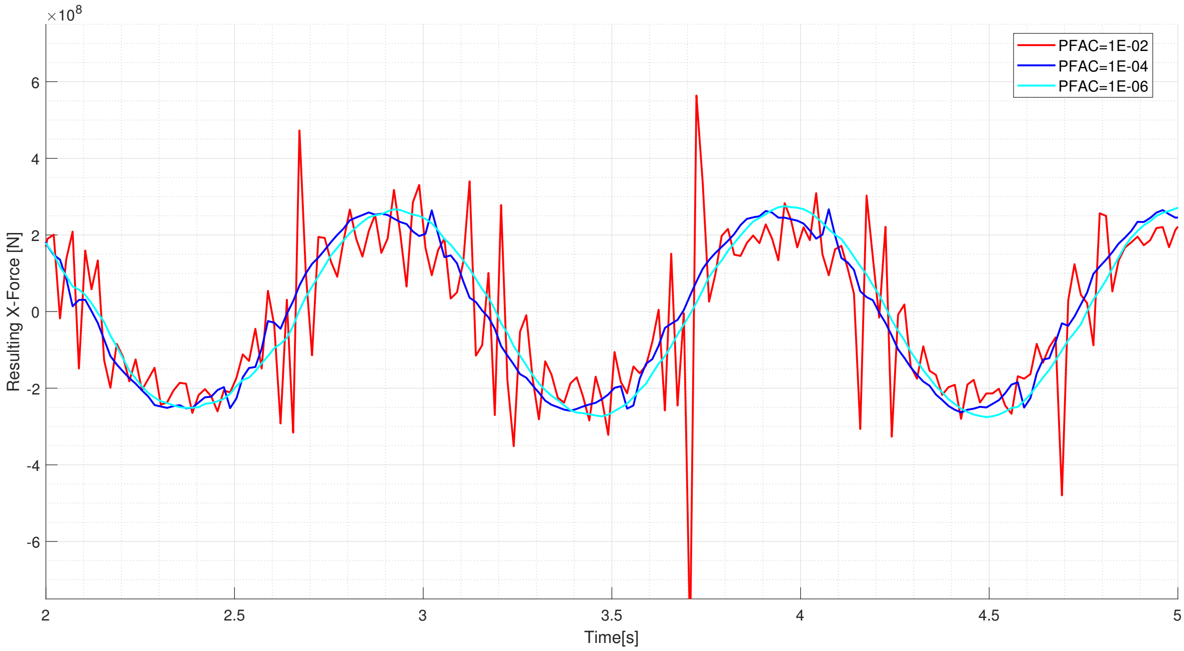

Figure 11: Surge direction force history on oscillating SPAR

PFAC values within the range of 1×10^{-4} - 2×10^{-4} seem to give the most reasonable results (closer to values from BEM) in terms of water added mass. But, increasing the values of PFAC to values greater than 1×10^{-4}, also leads to a stiffer coupling, resulting in an oscillating FSI force. Since an over-stiff coupling could lead to abrupt drop in time-step and numerical instabilities, the value of 1×10^{-4} is finally chosen for FSI coupling of the SPAR.

5.3 Bow Wave

An imaginary OSV of 3190 tons DWT is used as the striking ship. The hull geometry and main particulars are shown in figure-12 and table-3 respectively.

Table 3: Main particulars and mass properties of striking ship

L	75.9 m
L_{wl}	70.33 m
B	15.72 m
T	4.8 m
Δ	3190.6 tons
COG (x,y,z)	(31.42,0,0.4) m
COB(x,y,z)	(31.42,0,-1.9) m
I_{xx}	$3.901 \times 10^7\ kg.m^2$
I_{yy}	$1.840 \times 10^{10}\ kg.m^2$
I_{zz}	$1.836 \times 10^{10}\ kg.m^2$

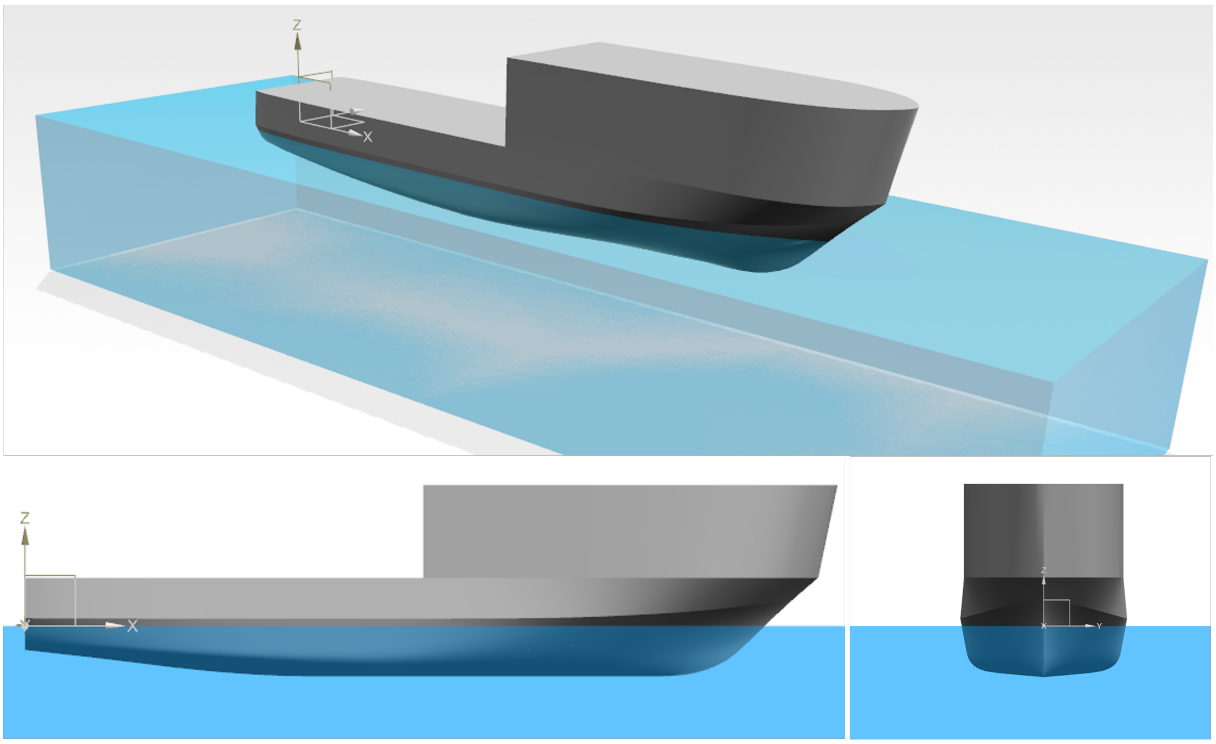

Figure 12: Geometry of reference OSV used for collision

As shown in figure-12, the origin for the coordinate system is located at the stern end of the vessel and intersection of waterplane with the vertical plane of symmetry. The inertia properties reported in table-3 are measured with respect to the COG.

To validate the bow wave generated by the hull, the free surface elevation results obtained from

LS-DYNA simulations are compared to those obtained from the potential flow solver REVA (calculations in REVA were performed by associate professor Lionel GENTAZ from Ecole Centrale Nantes). In LS DYNA ALE, the ship is constrained in all DOFs except surge. The hydrostatic pressure in the fluid domain is allowed to develop over a duration of 0.5 seconds. At 0.8 seconds the ship is given a velocity in surge direction. The velocity is increased to its maximum value over a duration of 1 second and held constant thereafter. The shape and height of the bow wave at different time instants are then visually inspected. Time history of the net resistance force acting on the hull is used as an indicator to estimate the travel length and time for the ship before a stable flow field is formed. It is observed that the default value of 0.1 for PFAC leads to an over-stiff coupling. Moreover, the flow around the hull is tangential, whereas the coupling forces push the water in a direction normal to the hull. Hence, a high coupling stiffness produced unrealistic results with respect to the bow wave. Tracer nodes were placed ahead of the bow to track water particle location during the simulation. The z-displacement of this tracer is observed to quantitatively measure the height of the bow wave. The tracer node also provides data about the x-coordinate and velocity of water particle. But, due to the nature of penalty coupling acting in a direction normal to the hull surface, the kinematic quantities in the longitudinal direction cannot be compared. Figure -13 shows a comparison of the free surface elevation at the bow obtained from LS-DYNA/ALE compared to the results from REVA. According to Prof. Lionel Gentaz, the potential flow solver REVA relies on linearization of the free surface and as a result, the bow wave crest could be underestimated.

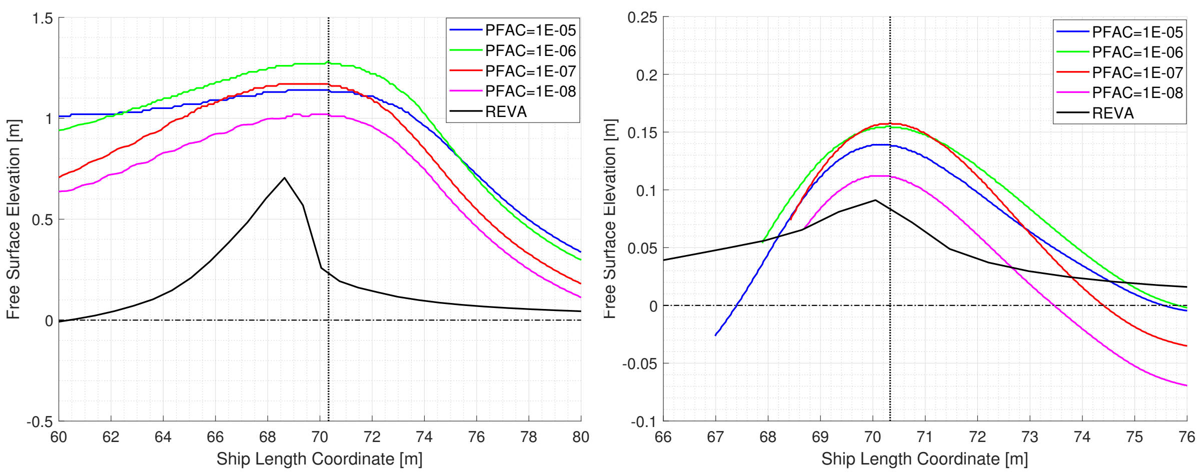

(a) Ship Speed = 5 m/s (b) Ship Speed = 2 m/s

Figure 13: Free Surface Elevation from LS-DYNA/ALE and potential flow solver REVA

It must be noted that in figure-13, the longitudinal position of the free surface elevation obtained from REVA is more accurate, whereas in LS-DYNA/ALE, the exact longitudinal position with respect to the hull could not be measured. The free surface elevation plots were generated by assuming that the fluid particles in LS-DYNA/ALE have a constant longitudinal velocity equal to the ship speed. In all LS-DYNA/ALE simulations, the crest of the bow wave is higher than the potential flow solver results. The peak of the crest in LS-DYNA/ALE is formed ahead of the hull rake intersection with the still water line, whereas in REVA, the crest peak occurs slightly behind this intersection point.

The wave profile generated in LS-DYNA/ALE for a ship speed of 5 m/s, after 5.5 seconds of ship travel is shown in figure -14

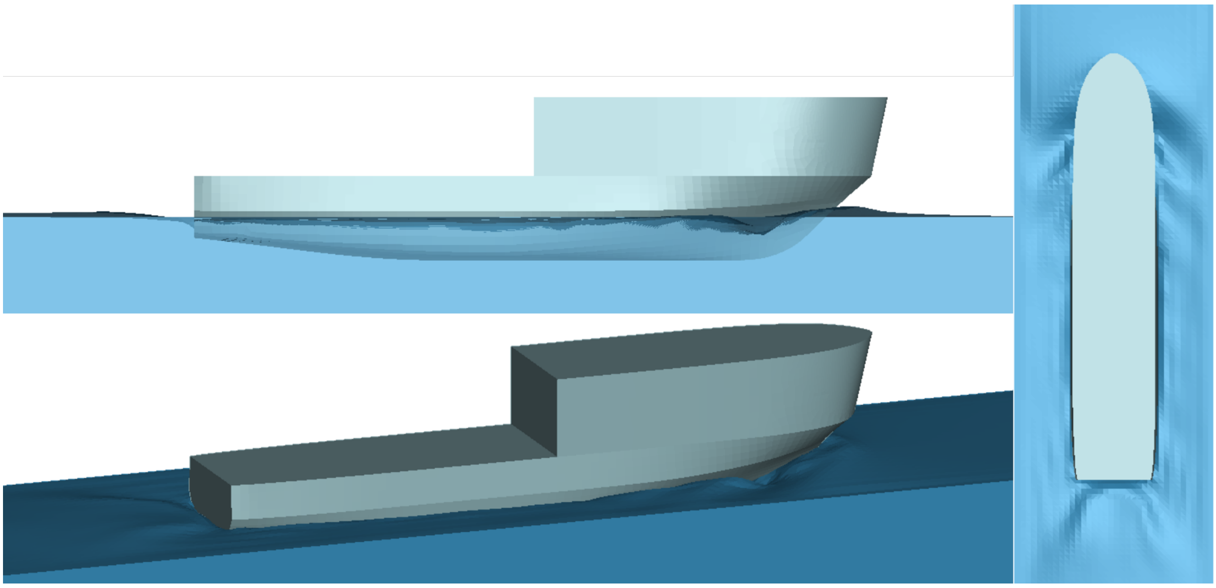

Figure 14: Wave profile from LS-DYNA/ALE for a ship speed of 5 m/s

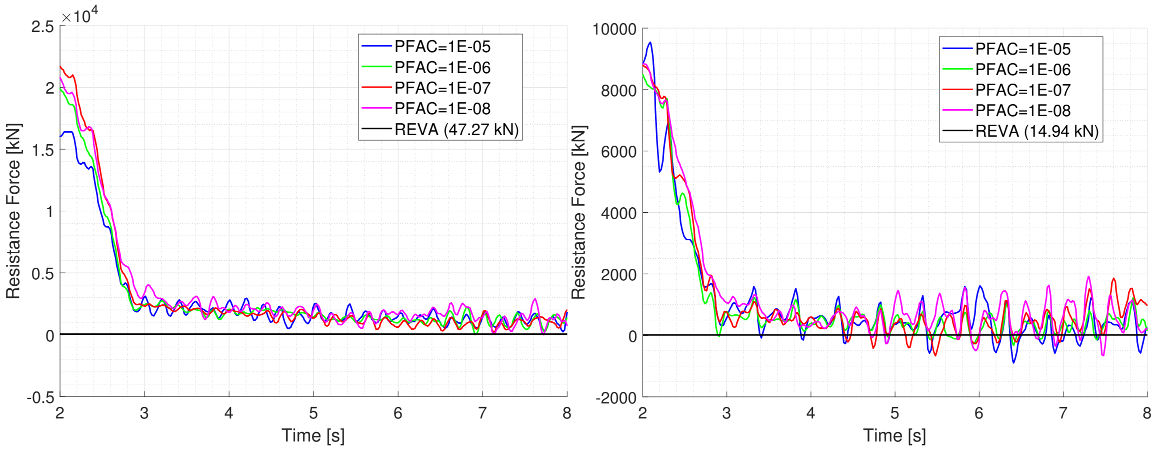

(a) Ship Speed = 5 m/s

(b) Ship Speed = 2 m/s

Figure 15: Resistance Force from LS-DYNA/ALE and potential flow solver REVA

Figure-15 shows that the resistance force in LS-DYNA/ALE is oscillatory and enormously overestimated compared to the results from REVA. The ship travel in the final collision event is limited to 6 seconds to preserve the numerical stability of FSI forces on the ship.

5.4 Errors in Fluid-Structure Interaction

From the initial simulations to validate the fluid structure interaction, the following conclusions can be drawn.

1. An indefinitely stable hydrostatic equilibrium cannot be reached for the floating structures, because there is always some leakage of water into the structures, irrespective of the PFAC values used.

2. The added mass effect is dependent on the PFAC value used. Using the PFAC value which yields added mass closer to BEM values, results in the FSI forces being highly oscillatory, indicating an over-stiff coupling.

3. Using the values of PFAC to obtain a reasonable added mass effect, always overestimates the drag coefficients.

Some possible reasons for the errors are discussed below

Artificial Added Mass Effect: The CEL approach uses a partitioned solver which is based on a loose coupling between the fluid and structure. As described by Förster et al. (2007) & Thavornpattanapong et al. (2011), the sequentially staggered coupling algorithm for FSI problems is inherently unstable. The fluid-structure interface is used as the boundary to solve the governing equations of the fluid. With time marching schemes, errors in construction of the fluid-structure interface are propagated to the next time step and add to the instability of the solution. The effect of fluid viscosity, structural stiffness and time-step size also play a role in numerical stability of the solution. Increasing the structural stiffness has a slightly positive effect on numerical stability. It is stated that decreasing the time step has a negative effect on the numerical stability. The authors also conclude that during the initial stages of the simulation, the onset of numerical instabilities can be approximated. Whereas, as the simulation proceeds in time, the effect of structural, geometric and material non-linearity become more dominant. This makes it almost impossible to accurately determine the onset of numerical instabilities.

Interface Reconstruction: The added mass effects result from the pressure in the fluid-structure interface. To accurately represent these forces, it is necessary that the interface between the fluid and structure is properly defined throughout the simulation. It can be observed from figure-16, that the initial interface between the lagrangian mesh and the fluid mesh is not properly constructed. The blue region represents the water and the red region represents air outside the SPAR. The green region is the air filled inside the SPAR, which must be prevented from leaking out. This error in interface reconstruction, particularly at the free surface could lead to errors in diffraction effects occurring at the free surface. Mesh refinement can help in more accurate initial interface construction, but also leads to additional computational efforts.

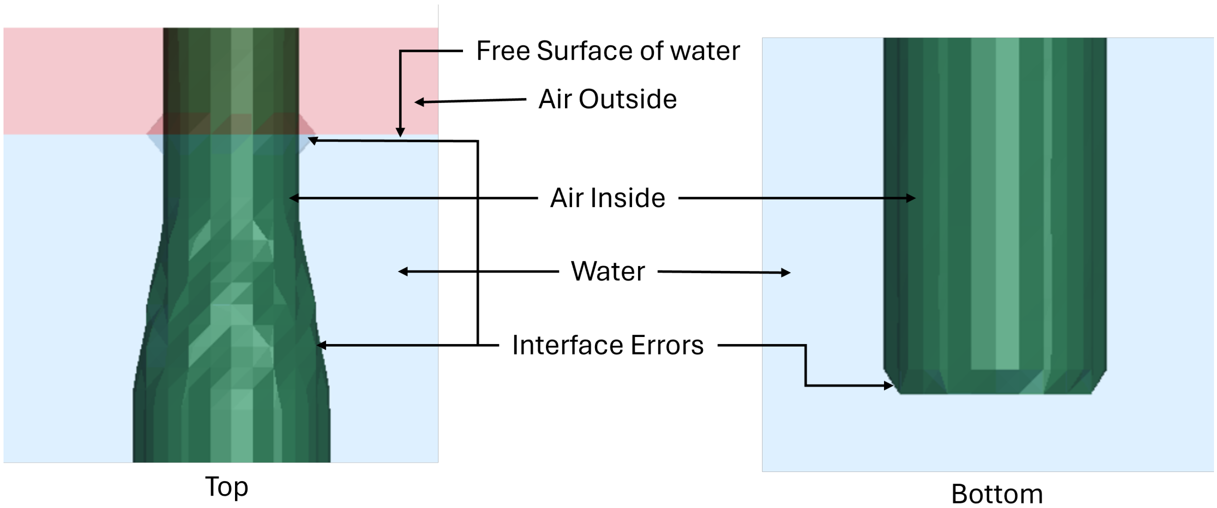

Figure 16: Fluid-Structure Interface for the SPAR

Effect of Hydrostatic Pressure: In reality, the added mass force is an inertial force resulting purely from the fluid motion. Hence, the hydrostatic pressure in the fluid does not affect this force. But, in the CEL approach, the total penalty coupling pressure is responsible for avoiding fluid penetration into the structure. Hence, this coupling pressure must also include the hydrostatic pressure in the fluid. For the SPAR with a draft of 120 m, there is a drastic variation in hydrostatic pressure along the depth.

6 COLLISION EVENT SIMULATIONS

6.1 Simulation Setup

The primary aim of this thesis is to compare the CEL approach using LS-DYNA/ALE and a simplified method using LS-DYNA/MCOL. The effect of mooring lines are ignored. Since the focus of this research is on the damage to the FOWT, the striking ship is assumed to be a rigid body. The collision events are simulated for two different ship speeds of 5 m/s and 2 m/s. The different simulation setups, along with the name used for comparison of results, are explained below. In all the following simulations, the sway, roll and yaw DOFs are constrained for both the striking ship and the FOWT. This is based on the assumption that, for a head-on collision, the problem remains symmetric about the longitudinal vertical plane (Y = 0).

LS-DYNA/MCOL Simulations

For MCOL simulations, the ship is prescribed an initial velocity before impact. The ship is placed close to the FOWT such that there are no initial penetrations between both structures.

M:SPAR - MCOL boundary condition is enabled only for the FOWT. The ship is constrained in all DOFs except surge. The striking ship is treated as an object with a Constant Added Mass (CAM), by including the hydrodynamic added mass to its total rigid body mass.

M:SPAR+SHIP - MCOL boundary condition is enabled for the FOWT as well as the striking ship. Unlike CEL simulations, the travel of the ship is not included and the gravity load is not explicitly modelled. Hence, there is no need to constrain the different DOFs of the ship. Moreover, it was noticed that the use of MCOL boundary condition in the simulation, overwrites any other prescribed boundary condition applied to the same rigid body.

CEL Simulations (LS-DYNA/ALE)

Unlike LS-DYNA/MCOL simulations, modelling the collision event using LS-DYNA/ALE presents an additional challenge. In the validation studies, it was noted that an indefinitely stable hydrostatic equilibrium could not be achieved for the SPAR. This leads to the FOWT sinking over the duration of ship travel. The resulting point of impact and penetration trajectory differ based on the boundary conditions applied to the ship and FOWT. Different simulations with varying boundary conditions on the ship and SPAR are performed to investigate the effect of applied boundary conditions.

S:SPAR - FSI coupling using LS-DYNA/ALE is applied only to the FOWT. The striking ship is modelled using CAM approach similar to the simulation setup of **M:SPAR**. Gravity loads are applied on all parts except the striking ship. Heave DOF of the FOWT is held fixed during the ship travel and released at the instant before impact.

S:SPAR (Noheave) - FSI coupling using LS-DYNA/ALE is applied only to the FOWT. The striking ship is modelled using CAM approach similar to the simulation setup of **M:SPAR**. The ship is constrained in all DOFs except surge. The surge and pitch DOFs are allowed and heave is fixed for the FOWT throughout the simulation, this preventing it to sink.

S:SPAR+SHIP - Both the striking ship and FOWT are coupled using LS-DYNA/ALE. Heave DOF of the FOWT & heave and pitch DOFs of the striking ship, are held fixed during the ship travel and released at the instant before impact.

S:SPAR+SHIP (Noheave) - Both the striking ship and FOWT are coupled using LS-DYNA/ALE. The heave DOF for both the striking ship and struck FOWT are held fixed throughout the simulation. The pitch DOF of the striking ship is held fixed during ship travel and released before impact occurs.

The extent of fluid domains used for CEL simulations are shown in figure-17. An example keyword file used to define the fluid domain for S:SPAR+SHIP is shown in Appendix-B.

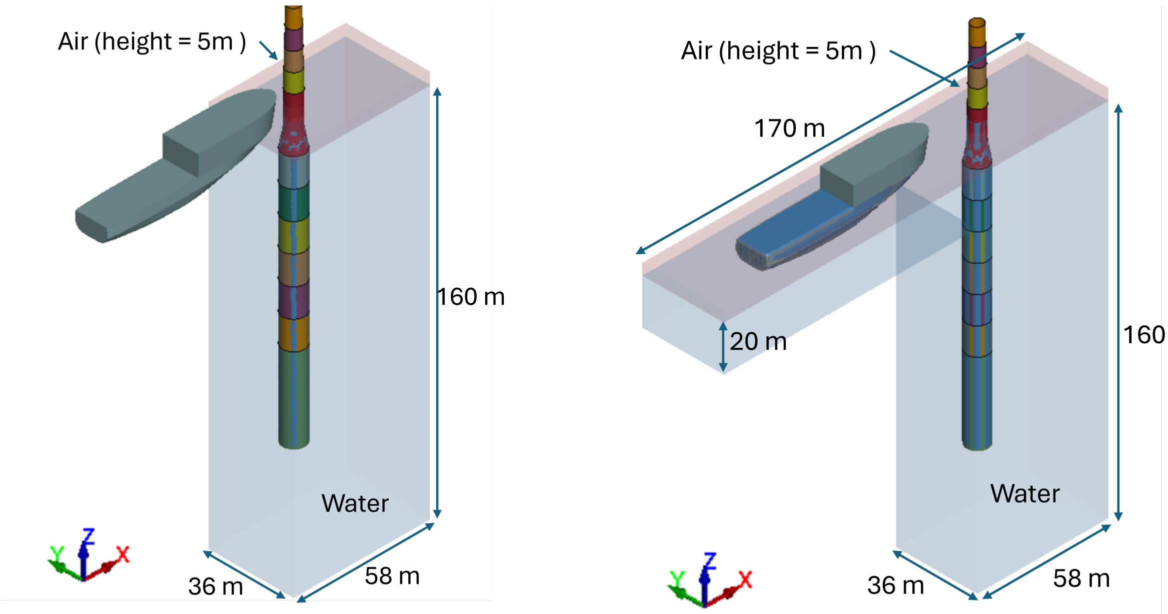

(a) S:SPAR & S:SPAR (Noheave) (b) S:SPAR+SHIP & S:SPAR+SHIP (Noheave)

Figure 17: Fluid domain used for CEL simulations

Table 4: Simulation setups and boundary conditions on Ship and FOWT : Fixed - DOF remains constrained for entire simulation; Free - DOF remains unconstrained for entire simulation; Released - DOF remains fixed during ship travel and is released just before impact

Simulation	SPAR						SHIP					
Name	Surge	Sway	Heave	Roll	Pitch	Yaw	Surge	Sway	Heave	Roll	Pitch	Yaw
M:SPAR	Free	Free	Free	Free	Free	Free	Free	Fixed	Fixed	Fixed	Fixed	Fixed
M:SPAR+SHIP	Free	Free	Free	Free	Free	Free	Free	Free	Free	Free	Free	Free
S:SPAR	Free	Fixed	Released	Fixed	Free	Fixed	Free	Fixed	Free	Fixed	Free	Fixed
S:SPAR (Noheave)	Free	Fixed	Fixed	Fixed	Free	Fixed	Free	Fixed	Fixed	Fixed	Fixed	Fixed
S:SPAR+SHIP	Free	Fixed	Released	Fixed	Free	Fixed	Free	Fixed	Released	Fixed	Released	Fixed
S:SPAR+SHIP (Noheave)	Free	Fixed	Fixed	Fixed	Free	Fixed	Free	Fixed	Fixed	Fixed	Released	Fixed

6.2 Energy Balance

MCOL

The energy balance calculated for **M:SPAR+SHIP**, with a ship velocity of 5 m/s is shown in figure-18. It must be noted that, to achieve a complete energy balance, the kinetic energy of the nodes undergoing deformations must also be accounted for in K_{ship} & K_{FOWT} (Ladeira et al. 2023). The total energy measured from **GLSTAT** in LS-DYNA, includes the wet kinetic energy (kinetic energy including the hydrodynamic added mass) of the parts coupled to MCOL and the kinetic energy of the deformed nodes. But the work done by viscous, wave damping and hydrostatic forces are not included. Hence, to calculate the correct total energy, the work done by fluid forces ($E_{hydro} = \Sigma W_{hydrostatic} + W_{viscous} + W_{radiation}$) must be added to the total energy measured from **GLSTAT**. The kinetic energy of the striking ship and the struck FOWT are measured from the **mcol** file output (wet ship kinetic energy, which includes the effect of water added mass should be considered).

From figure -18, it can be seen that approximately 95 % of the kinetic energy of the striking ship (including the water added mass), is distributed as the deformation energy and kinetic energy of the struck FOWT. It can also be seen that the total internal energy of the struck FOWT continues to increase. On further investigation, it was observed that additional plastic deformation was induced due to the motion of the Rotor Nacelle Assembly (RNA). The effective plastic strain observed in vicinity of the RNA, at $t = 2s$ and $t = 4s$ after impact are shown in figure-19

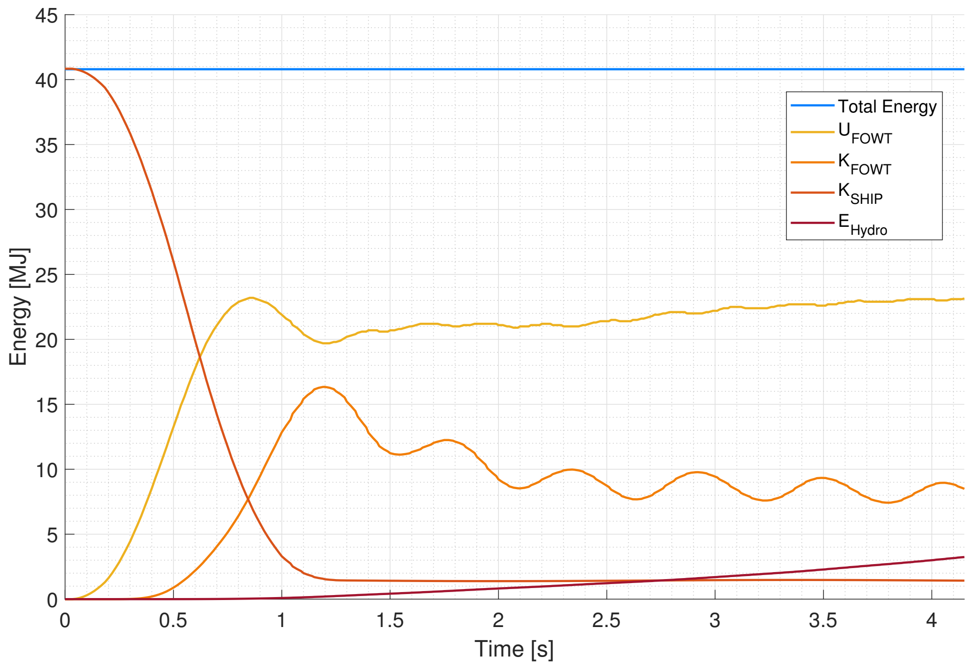

Figure 18: Energy balance for M:SPAR+SHIP with ship speed = 5 m/s

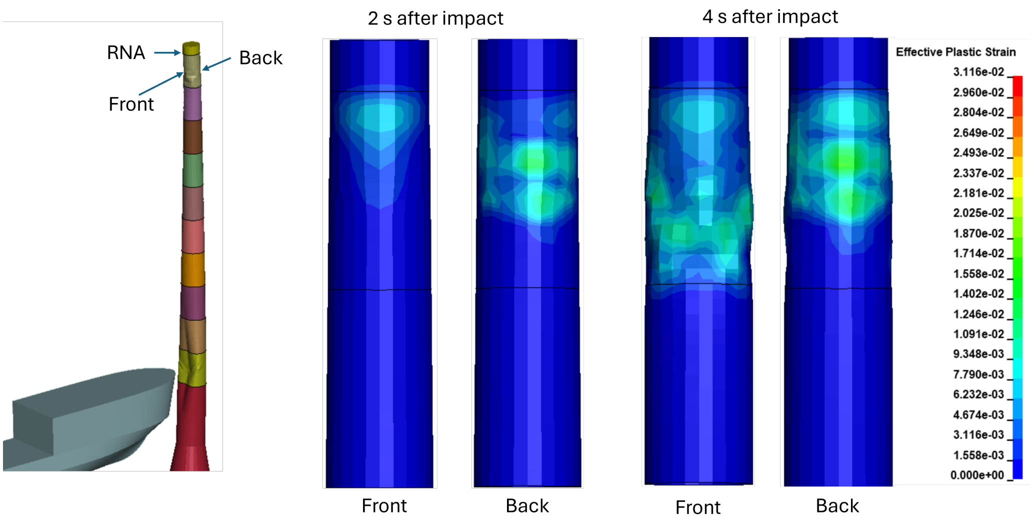

Figure 19: Effective plastic strain at RNA (M:SPAR+SHIP with ship speed = 5 m/s)

LS-DYNA/ALE

For CEL simulations using LS-DYNA/ALE, a complete energy balance could not be calculated due to the following reasons

1. The simulation domain includes ambient elements. The energy associated with these ambient elements could not be separately calculated.

2. The internal energy in MCOL simulations only refers to the internal energy of the structures, whereas in ALE formulation, air and water have an internal energy associated with their respective equation of state.

3. The gravity load is imposed over a duration of 0.5 seconds. Over this period, the fluid domain gains kinetic energy while also interacting with the ambient elements. Hence, the amount of energy transferred between the fluids and the ambient environment cannot be accurately accounted for in the energy balance.

4. The advection step in ALE may cause artificial energy dissipation. A large negative sliding work was observed in CEL simulations. The exact cause of this negative sliding work, needs further investigation.

6.3 Comparison of Results

NOTE:*For all the following comparisons, the values from* ***M:SPAR*** *are used as reference to calculate the % difference.* $t = 0$ *represents the instant of impact. The time shown in negative represents the period of ship travel before impact*

6.3.1 Contact Force

Figure-20, shows the time evolution of contact force in the surge direction during the collision. Both MCOL and CEL approaches predicted the same forces for the first 0.2 seconds. In all MCOL simulations, the energy and momentum transfer between the striking ship and FOWT occur over a single contact. In CEL simulations, only a single contact is observed for a ship speed of 2 m/s; whereas for a ship speed of 5 m/s, multiple contacts are observed. When both the striking ship and FOWT are coupled using CEL approach and the heave DOF is constrained, the predicted contact force is highest. The discrepancies observed can be explained by investigating the rigid body motions (section-6.3.4).

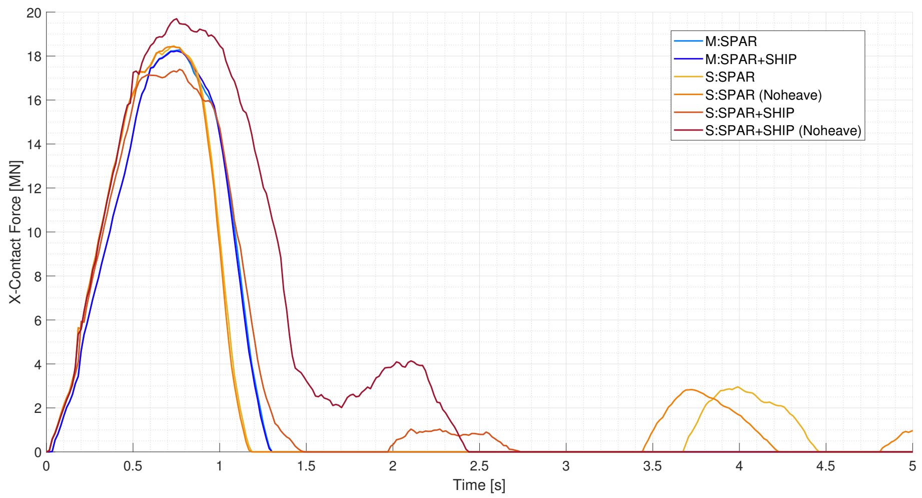

(a) Ship Speed = 5 m/s

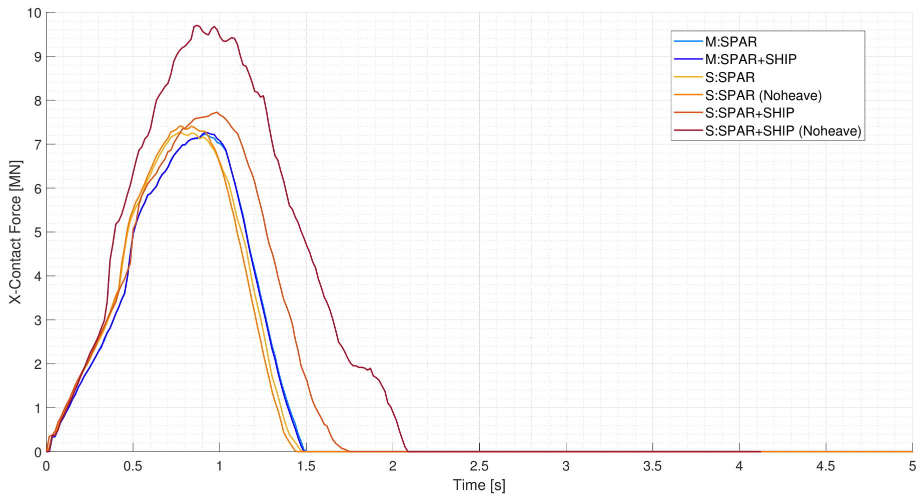

(b) Ship Speed = 2 m/s

Figure 20: Time history of contact force in X-direction

6.3.2 Penetration

The change in X-length between a node on the struck face of the FOWT and a node lying circumferentially opposite to this point, is used as a measure of penetration. The time history of penetration, shown in figure-22 is coherent with the observation made on the contact forces. For CEL simulation where both striking ship and FOWT are coupled and the heave DOF is constrained, the resulting penetration is the highest. The maximum penetration also occurs over a longer duration, same as the contact force.

Variations in penetration are observed even when contact forces are zero. This phenomenon is attributed to the global bending and elastic vibrations of the FOWT tower. The global deformation modes are significantly influenced by the presence of heavy masses at the RNA and the ballast.

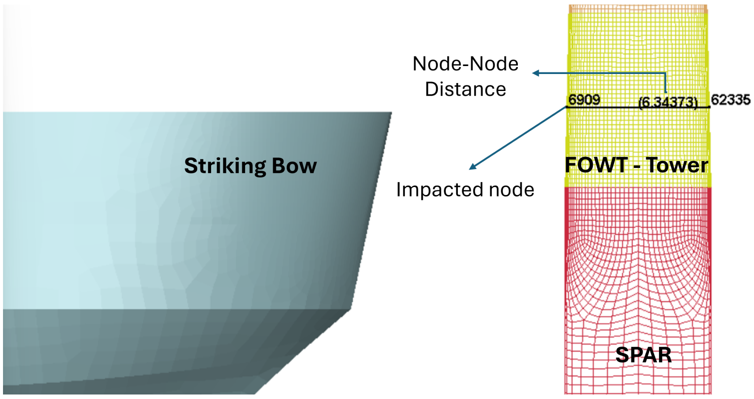

Figure 21: Node to Node distance used to measure penetration

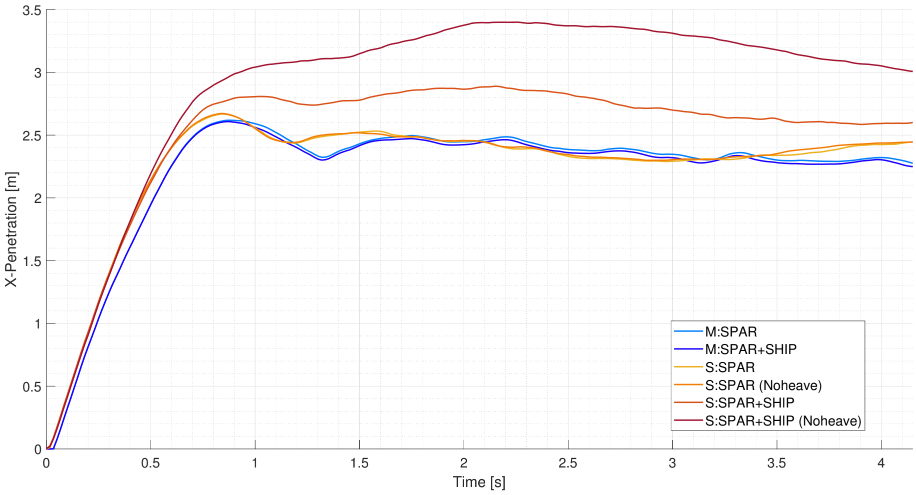

(a) Ship Speed = 5 m/s

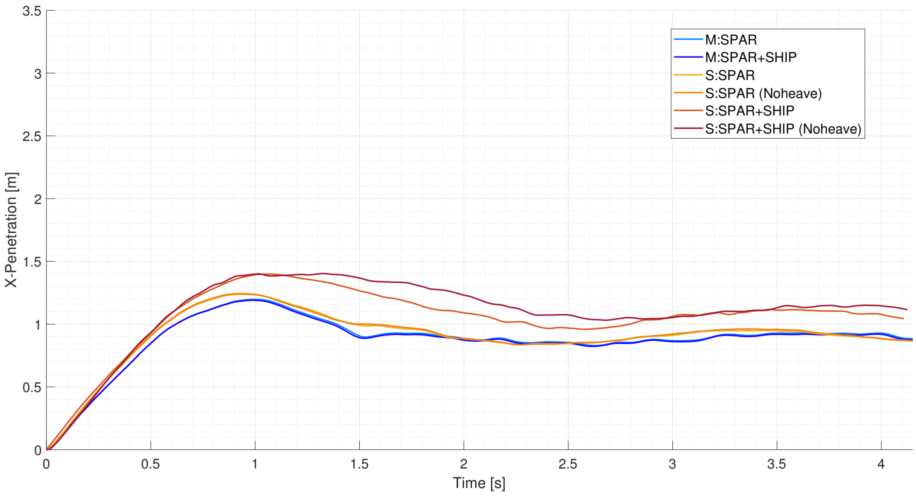

(b) Ship Speed = 2 m/s

Figure 22: Time history of penetration in X-direction

The deformed shape, at 2.5 seconds after impact is shown in figure-23. It can be observed that the shape and extent of deformation differs depending on the boundary conditions applied to the heave DOF.

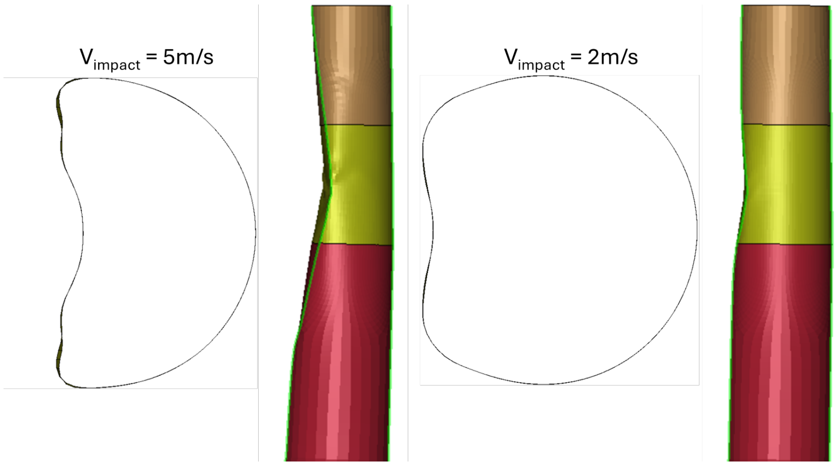

(a) M:SPAR

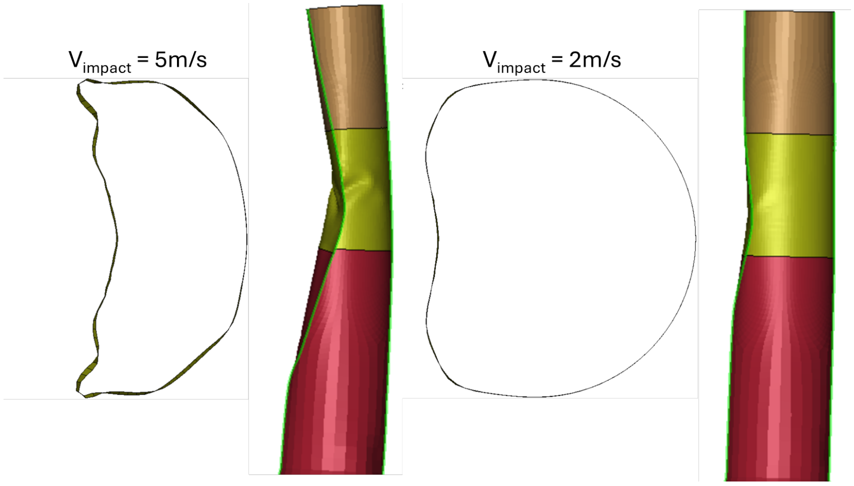

(b) S:SPAR+SHIP (Noheave)

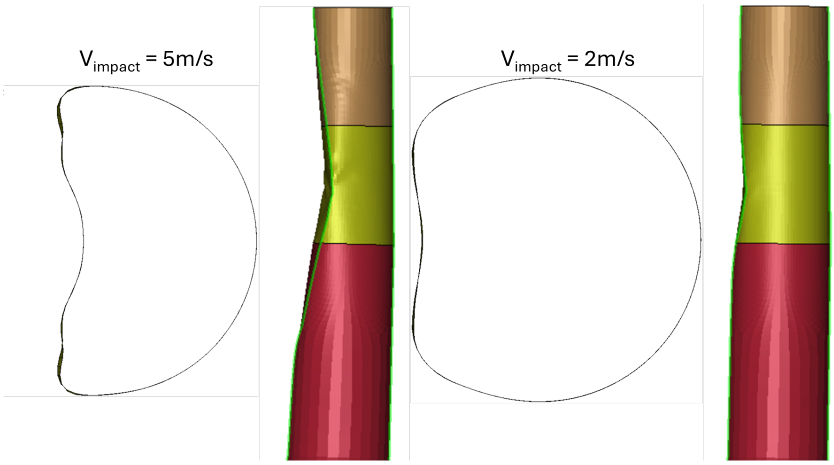

(c) M:SPAR+SHIP

Figure 23: Deformation profile of impacted region at 2.5 seconds after impact

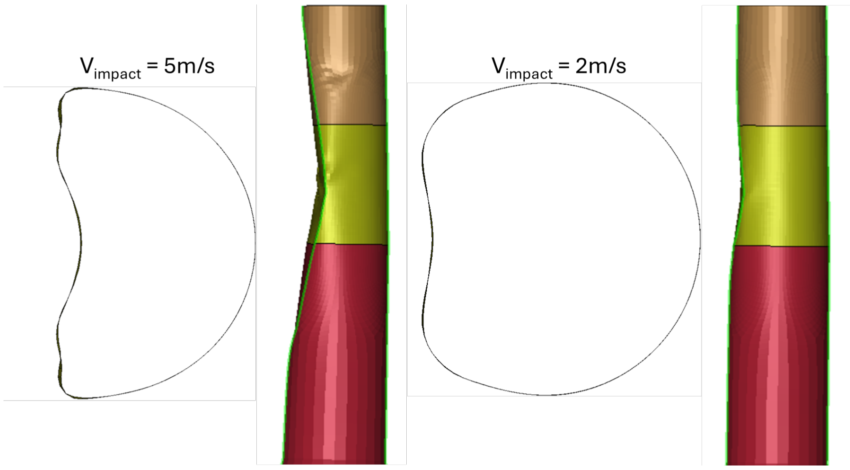

(d) S:SPAR (Noheave)

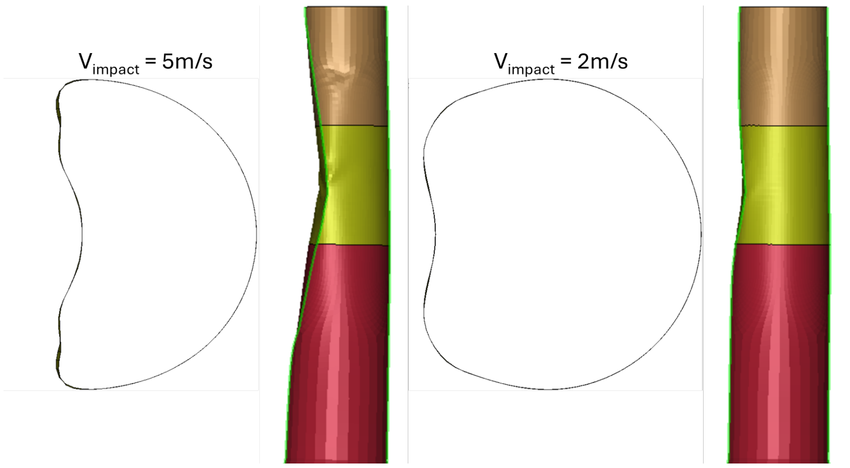

(e) S:SPAR

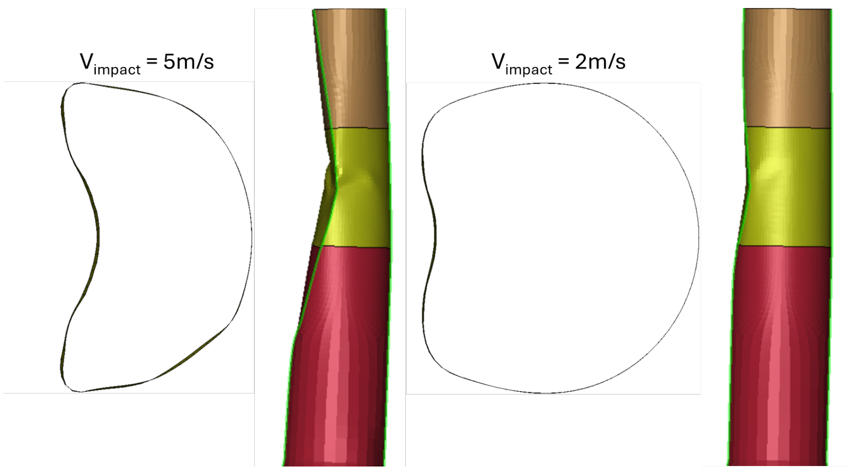

(f) S:SPAR+SHIP

Figure 23: Deformation profile of impacted region at 2.5 seconds after impact

6.3.3 *Deformation Energy*

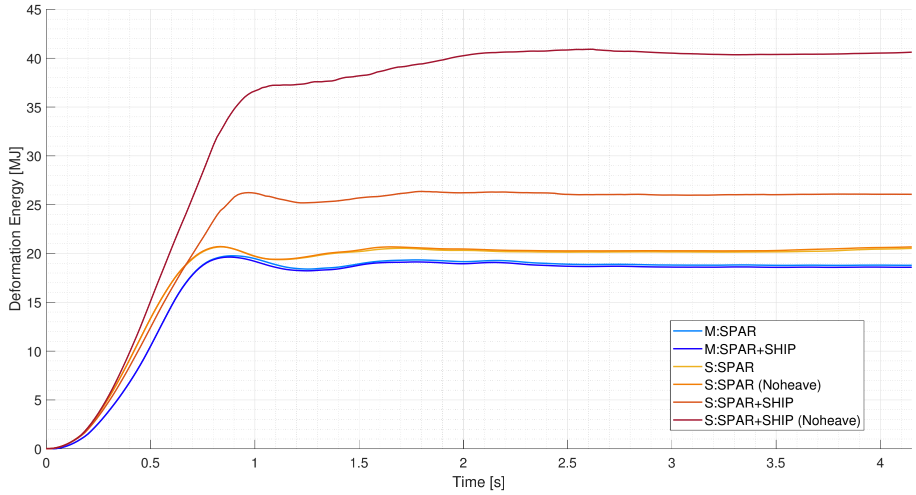

(a) Ship Speed = 5 m/s

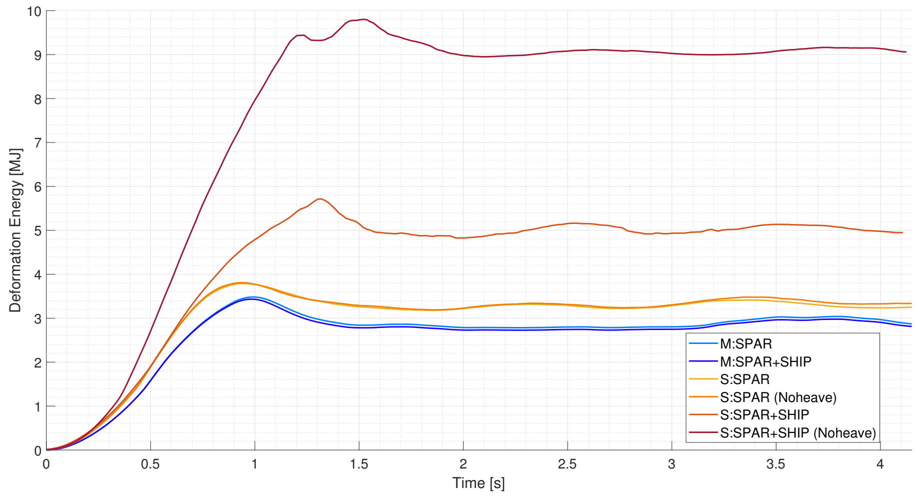

(b) Ship Speed = 2 m/s

Figure 24: Time evolution of impacted parts deformation energy

Table 5: Comparison of Damage to FOWT

Simulation	**Peak Contact Force [MN]**				**Deformation Energy [MJ] @ t=2s**				**Maximum Penetration [m]**			
Name	V_{impact} **= 5m/s**		V_{impact}**= 2m/s**		V_{impact} **= 5m/s**		V_{impact}**= 2m/s**		V_{impact} **= 5m/s**		V_{impact}**= 2m/s**	
M:SPAR	18.282	0.00%	7.233	0.00%	19.167	0.00%	2.787	0.00%	2.618	0.00%	1.197	0.00%
M:SPAR+SHIP	18.231	-0.27%	7.273	0.57%	18.953	-1.12%	2.729	-2.07%	2.608	-0.39%	1.191	-0.54%
S:SPAR	18.462	0.99%	7.272	0.54%	20.320	6.01%	3.223	15.66%	2.668	1.88%	1.238	3.38%
S:SPAR (Noheave)	18.425	0.78%	7.411	2.47%	20.458	6.73%	3.230	15.89%	2.672	2.06%	1.243	3.84%
S:SPAR+SHIP	17.394	-4.85%	7.726	6.82%	26.223	36.81%	4.825	73.12%	2.889	10.35%	1.399	16.89%
S:SPAR+SHIP (Noheave)	19.697	7.74%	9.703	34.16%	40.272	110.11%	8.977	222.12%	3.400	29.85%	1.403	17.19%

A large difference in the total deformation energy after impact is observed between MCOL, and CEL simulations where both the ship and FOWT are coupled. The effective Von-Mises stress and the effective plastic strain of the impacted parts (figure-25), are compared between different simulations to explain the discrepancies. The results shown in figure-25 are at t=2.5 seconds after impact.

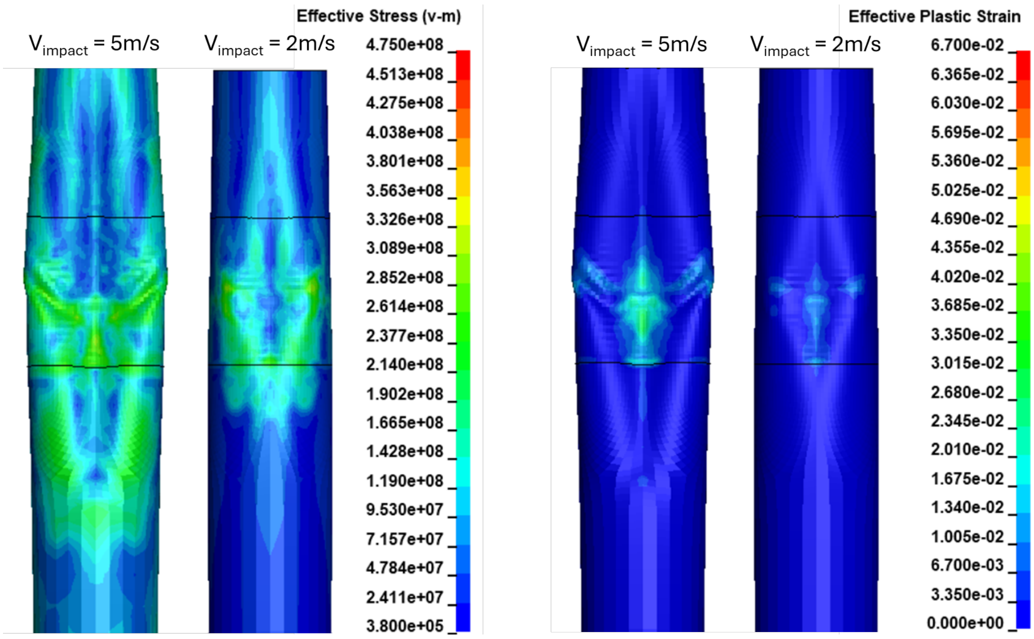

(a) M:SPAR

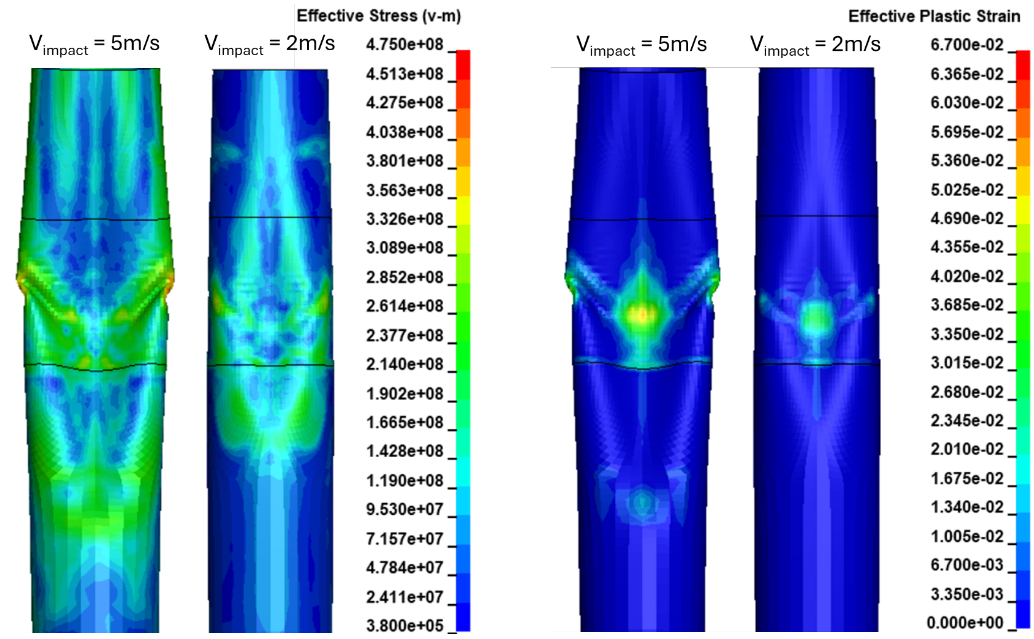

(b) S:SPAR+SHIP (Noheave)

Figure 25: Von-Mises Stress and Effective Plastic Strain

From figures -25a & 25b, a difference in extent of plastic deformation is observed. **M:SPAR**, shows lower stress levels compared to **S:SPAR+SHIP (Noheave)**. In the latter simulation, the plastic deformation is concentrated at the impact point and exhibits greater intensity. For a ship speed of 5 m/s, elevated strain levels are also detected along the sides, suggesting the initiation of a plastic hinge formation. This is responsible for the higher deformation energy of **S:SPAR+SHIP (Noheave)** observed in figure-24.

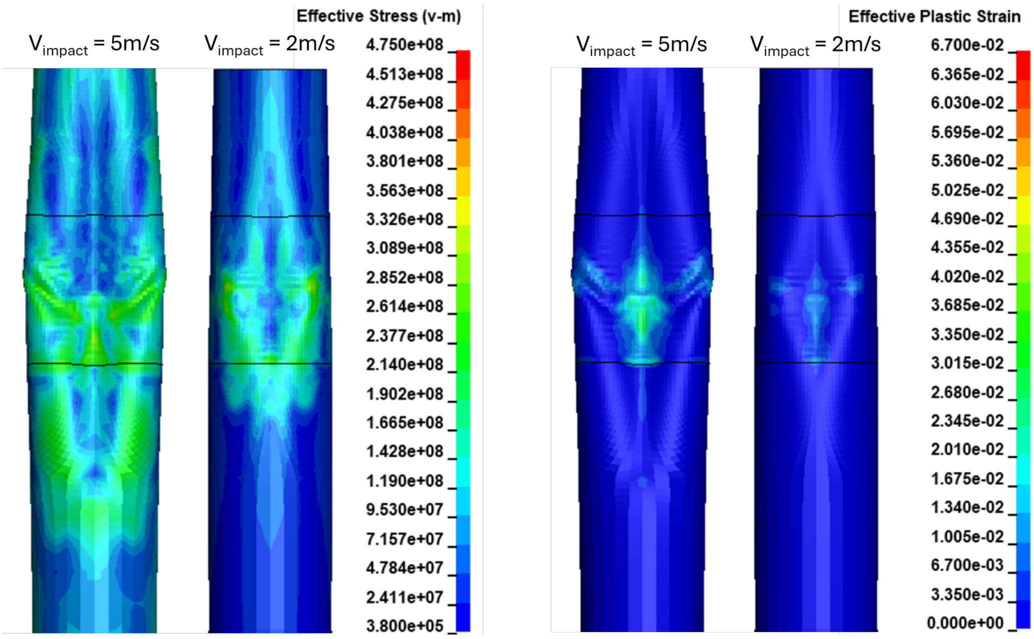

(c) M:SPAR+SHIP

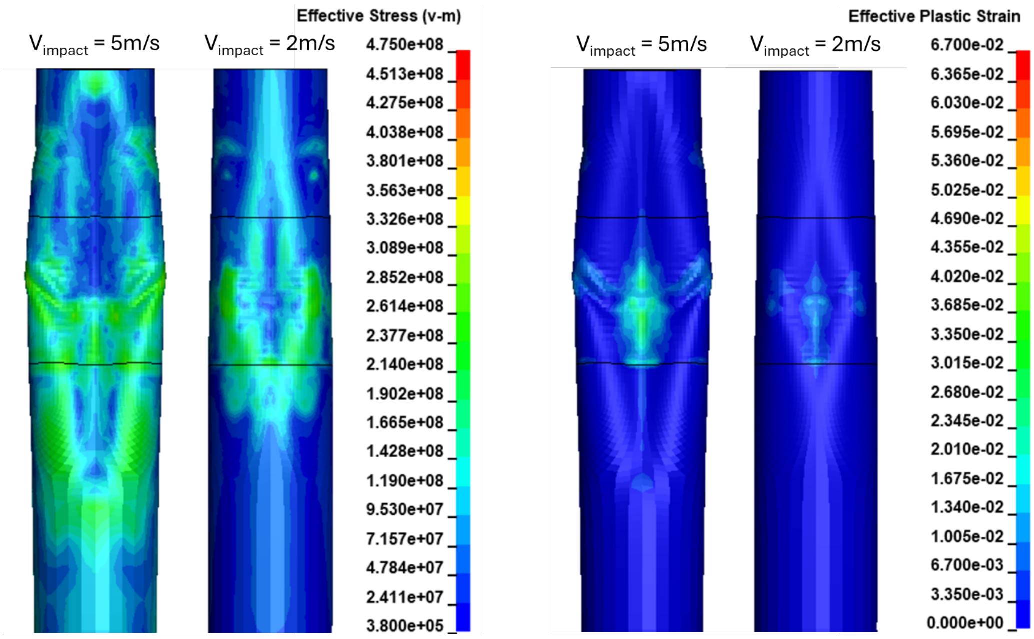

(d) S:SPAR (Noheave)

Figure 25: Von-Mises Stress and Effective Plastic Strain

Figures -25a, 25c & 25d, show that similar plastic deformations occur for **M:SPAR**, **M:SPAR+SHIP** & **S:SPAR (Noheave)**. This observation is coherent with the deformation energies shown in figure-24.

Changing the boundary conditions on heave DOF, affects the rigid body motions of the striking ship and/or the FOWT and hence the penetration trajectory as well as resulting damage area. This explains the difference observed between figure -25f and figure -25b.

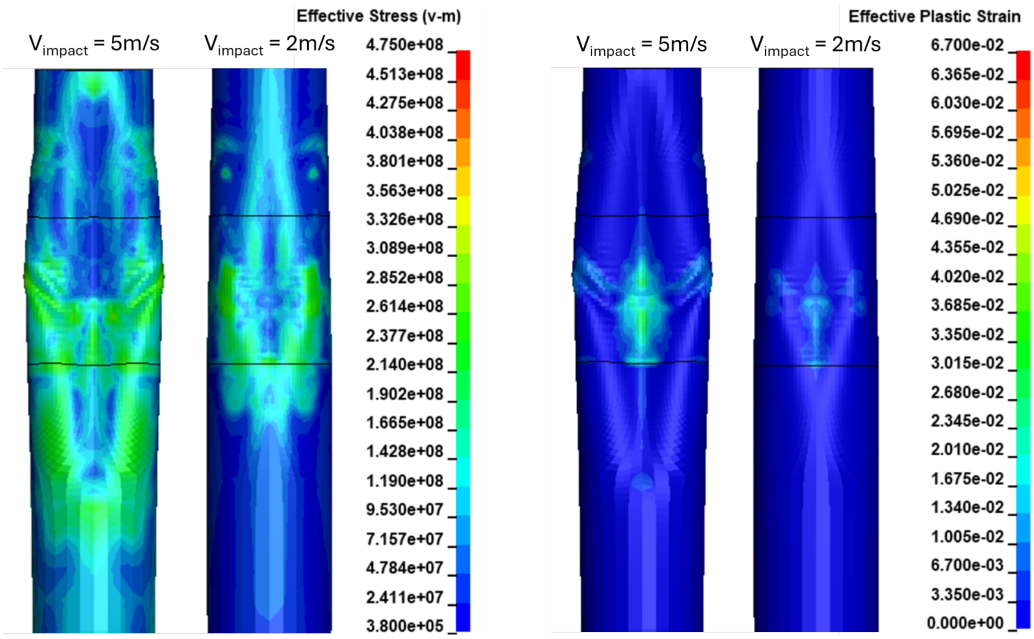

(e) S:SPAR

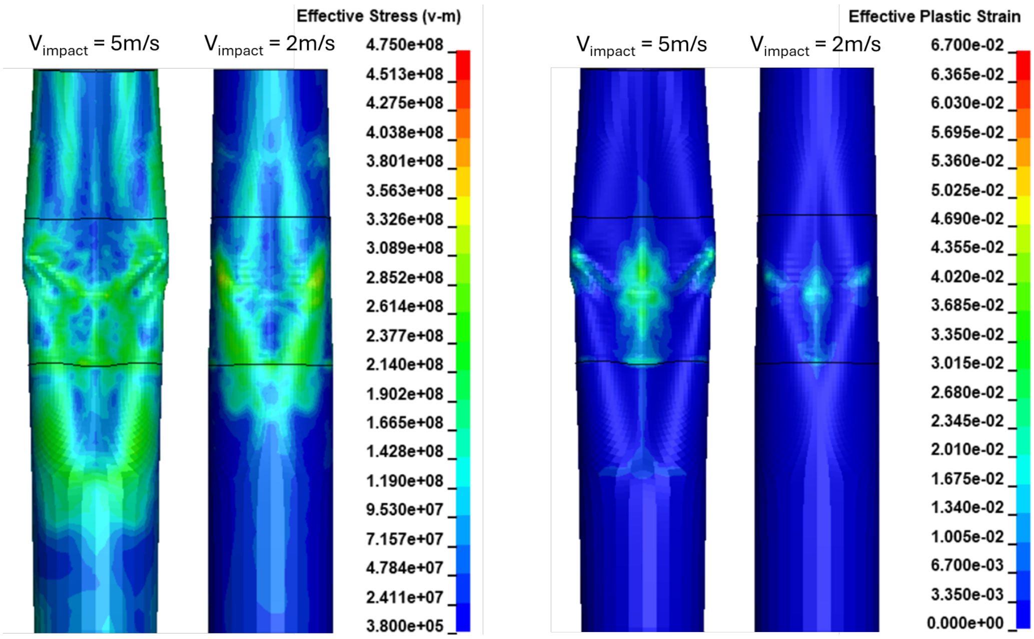

(f) S:SPAR+SHIP

Figure 25: Von-Mises Stress and Effective Plastic Strain

6.3.4 Pitch Angle & Surge Displacement of FOWT

The time evolution of the pitch angle and surge displacement of the impacted FOWT, before and after collision are shown in figure-26 & 27 respectively. Assuming small rotation of the SPAR, its initial metacenter is used as a reference point to measure the pitch and surge displacements. For CEL simulations where the striking ship is coupled to water (**S:SPAR+SHIP** & **S:SPAR+SHIP (Noheave)**), the generated bow wave influences the pitch and surge of the impacted FOWT. The effect of this bow wave is more pronounced for the pitch angle. The ship speed does not seem to influence the magnitude of this initial pitch angle due to the bow wave.

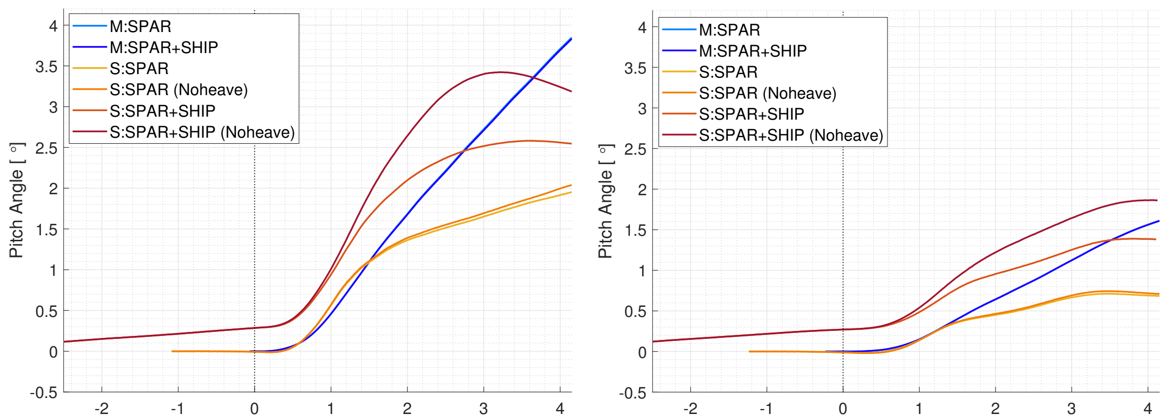

(a) Ship Velocity = 5 m/s (b) Ship Velocity = 2 m/s

Figure 26: Pitch angle of FOWT

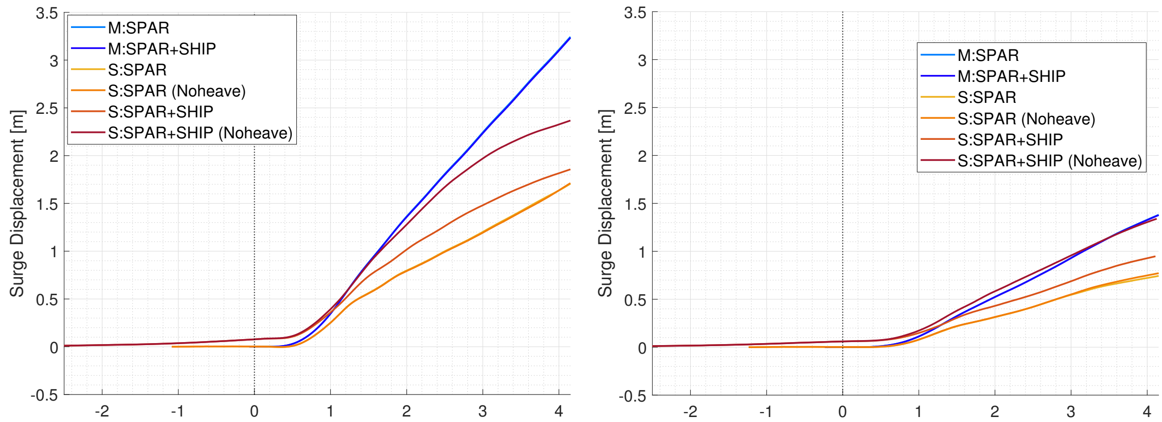

(a) Ship Velocity = 5 m/s (b) Ship Velocity = 2 m/s

Figure 27: Surge Displacement of FOWT

The time evolution of pitch and surge for the struck FOWT remains similar across all simulations up to approximately 0.5 seconds after impact. Beyond 0.5 seconds, the influence of Fluid-Structure Interaction FSI forces becomes more pronounced on the rigid body motions of both the struck and striking bodies, leading to differences in kinematic quantities between the simulations. In all CEL simulations, both pitch and surge displacements decrease more rapidly compared to MCOL simulations. The overestimation of FSI forces, as observed in the validation studies (section-5.2), can account for these differences. Additionally, the pitch angle is influenced by the hydrostatic restoring moment acting on the SPAR. In LS-DYNA/ALE, the restoring moment could not be accurately measured during the validation studies. However, given that the added mass and drag forces are overestimated, it is reasonable to expect a similar trend for the hydrostatic restoring moments due to the penalty coupling. This reasoning aligns with the observed behavior of the pitch angle after impact.

6.3.5 *Effect of Ship Wave & Kinematics*

The trajectory of penetration and the resulting damage to the Floating Offshore Wind Turbine (FOWT) are influenced by the kinematics of both the striking ship and the FOWT. These kinematics are, in turn, dependent on the applied boundary conditions. Figure-28 illustrates the penetration at different time instants after initial contact (t=0) for M:SPAR+SHIP and S:SPAR+SHIP (Noheave) simulations, with a ship speed of 5 m/s. The pitch motion of the striking ship differs between M:SPAR+SHIP and S:SPAR+SHIP (Noheave) simulations. In M:SPAR+SHIP, the striking ship is coupled using MCOL and is unconstrained in all degrees of freedom (DOFs). But, in S:SPAR+SHIP (Noheave), both the striking ship and FOWT are constrained in the heave DOF.

Figure-28b demonstrates the effect of surrounding water. Prior to impact, a small bow wave forms, causing initial pitch (Figure 26) and surge displacement (Figure 27) of the FOWT. As the striking ship moves, it generates a wake field. Upon impact with the FOWT, the ship decelerates, but the wake waves generated pre-impact continue to propagate at a velocity approximately equal to the initial ship speed. At 1.2 seconds post-impact, the effect of the stern wave becomes apparent. The following wake wave induces FSI forces on the stern of the striking ship, causing the bow to pitch downward. However, due to the constrained heave DOF, the ship's vertical displacement remains unaffected by the action of the following wave.

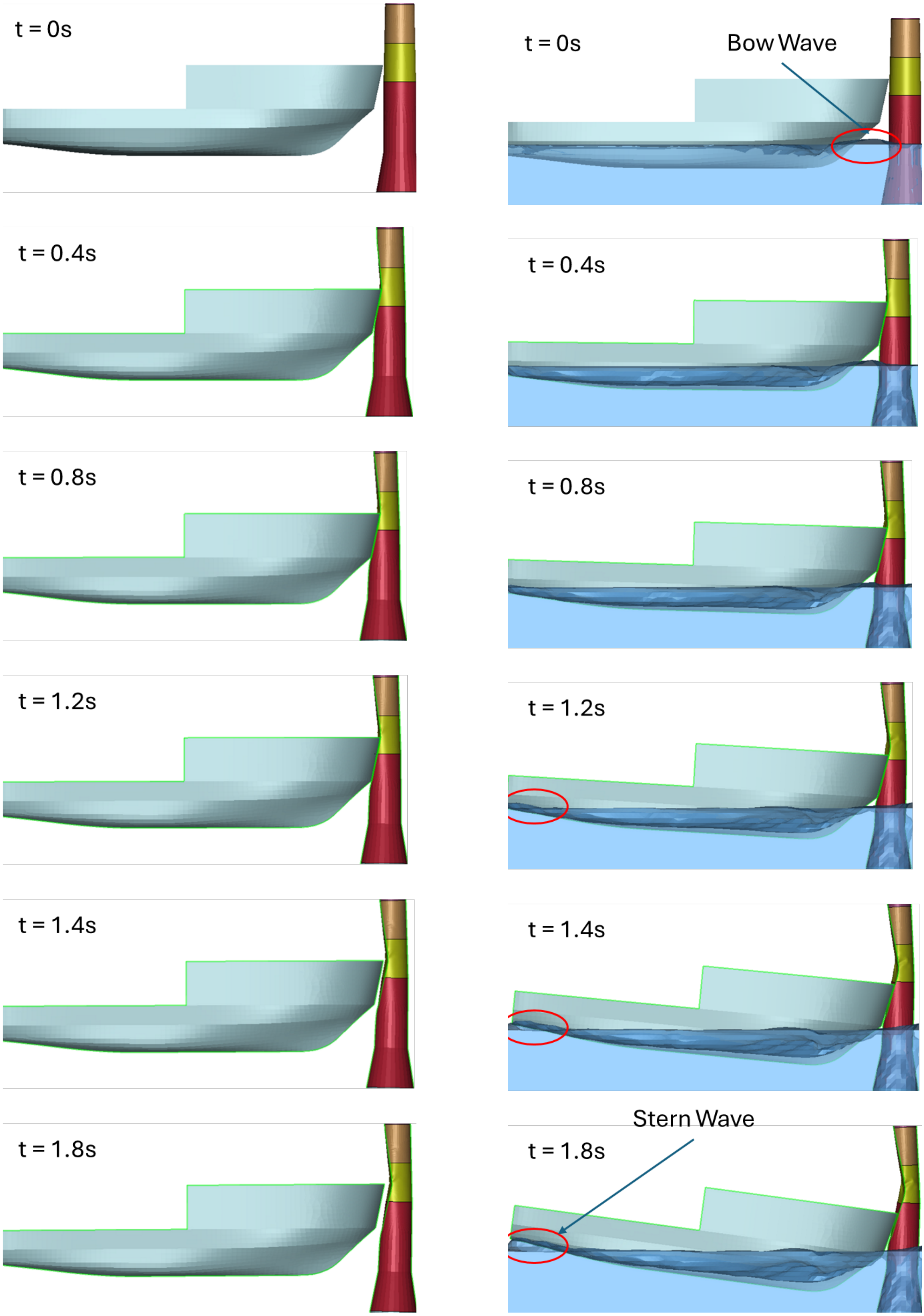

(a) M:SPAR+SHIP (b) S:SPAR+SHIP (Noheave)

Figure 28: Penetration Trajectory for ($V_{ship} = 5m/s$)

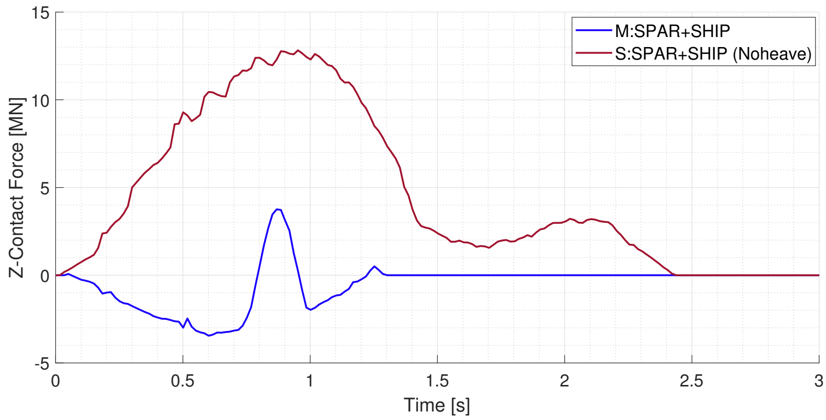

Figure 29: Z-Contact force ($V_{ship} = 5m/s$)

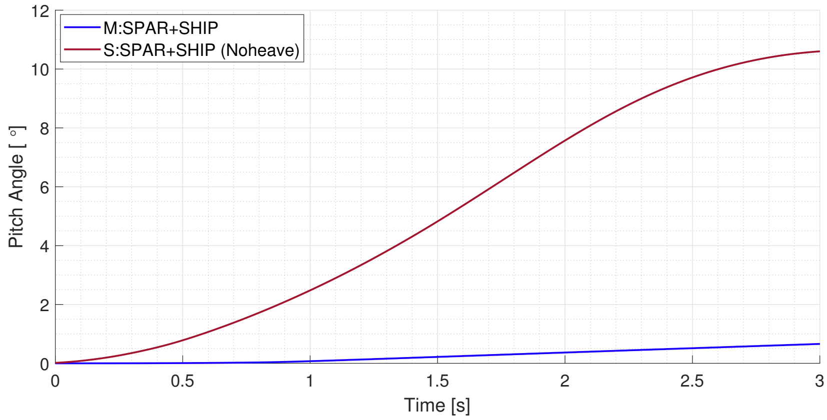

Figure 30: Ship Pitch ($V_{ship} = 5m/s$)

As the bow impacts the FOWT tower, a small amount of vertical contact force is generated in the contact region due to the rake angle of the bow. With the bow continuing to pitch downwards in S:SPAR+SHIP (Noheave), the vertical contact forces also increase (figure - 29 & 30). The FSI forces on the ship act in both the vertical (heave) and horizontal (surge) direction. Figure - 31 shows the horizontal FSI forces (surge direction) acting on the striking ship. The positive values in figure -31 refer to forces acting against the ship (negative global X direction).

While the vertical forces are responsible for the pitch motion, the horizontal forces (negative in figure - 31) continue to push the ship forward in surge direction. In M:SPAR+SHIP, the effect of fluid viscosity was not included and hence there are no fluid forces acting on the ship in horizontal direction.

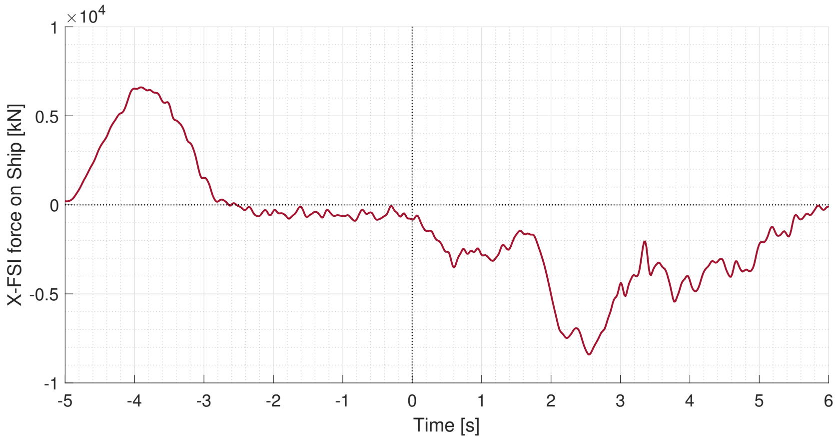

Figure 31: FSI forces on ship in surge for S:SPAR+SHIP (Noheave)($V_{ship} = 5m/s$)

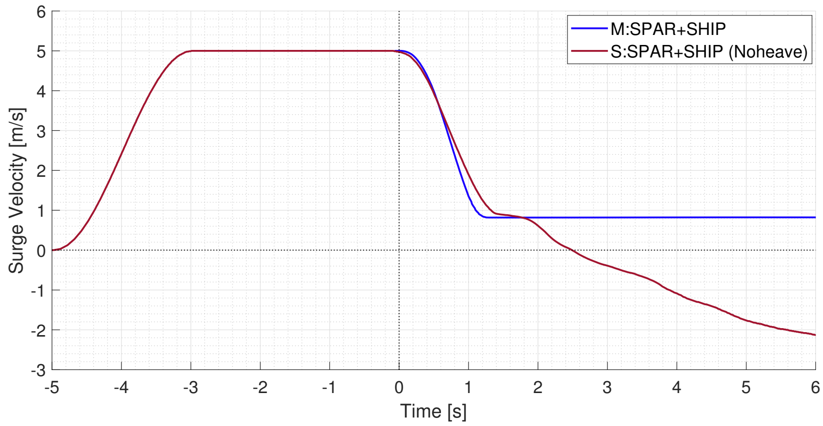

Figure 32: Ship surge velocity for S:SPAR+SHIP (Noheave)

In reality, the FOWT floats due to buoyancy and has no constraints on the heave DOF. Whereas in S:SPAR+SHIP (Noheave), an artificial constraint on the heave DOF is imposed to prevent sinking of the FOWT. This additional constraint, along with the pitch motion of the ship, leads to a penetration trajectory which is completely different from M:SPAR+SHIP and hence the resulting damage to FOWT tower is higher for S:SPAR+SHIP (Noheave).

Although the resulting difference between MCOL and CEL simulations can be explained, the effect of surrounding water in CEL simulations remains questionable. This is also evident from observations made on the horizontal FSI forces shown in figure -31 and the ship velocity after contact shown in figure -32. For the duration of ship travel with constant velocity ($t = -2$ s to $t = 0$ s), an unrealistic negative resistance force is observed. Similarly, at $t = 2.4$ seconds, there is a complete loss of contact and the ship continues to accelerate backwards (negative X direction). To further examine these FSI effects on the ship, the velocity vectors of the surrounding fluid are examined at different time instants before and after impact (impact occurs at $t = 0$ seconds). The velocity vectors are shown in figure -33.

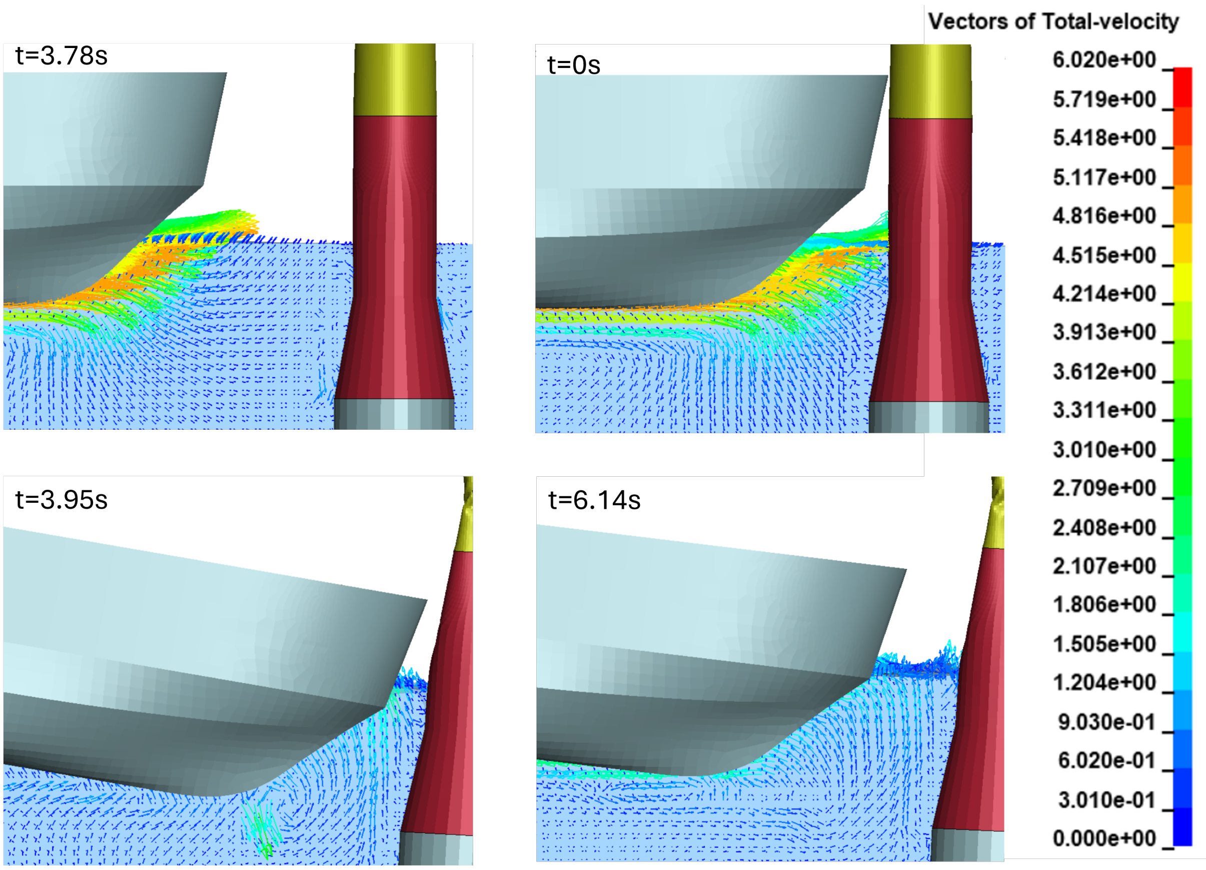

Figure 33: Velocity vectors of surrounding water for S:SPAR+SHIP (Noheave)($V_{ship} = 5m/s$)

After loss of contact, it can be seen that the water particles in vicinity of the ship bow obtain a velocity in the negative-X direction. This flow of water is responsible for accelerating the ship in the negative-X direction after loss of contact (figure -32). This phenomenon is obviously non-physical and needs further investigation.

7 CONCLUSION

The nature of FSI forces (hydrodynamic added mass) obtained using LS-DYNA/ALE was validated against results obtained from Boundary Element Method (BEM) solver - ANSYS AQWA. Similary, the bow wave generated in LS-DYNA/ALE was validated using the potential flow solver - REVA. The FSI forces obtained in LS-DYNA/ALE were overestimated by a large margin compared to BEM solvers. The CEL simulations using LS-DYNA/ALE presented some challenges with respect to modeling, which are discussed in section-7.1.

The results obtained between LS-DYNA/MCOL and LS-DYNA/ALE for the peak contact force and deformation energies are in good agreement when only the struck FOWT's FSI is modeled. Overestimation of FSI forces in LS-DYNA/ALE results in underestimation of rigid body motions of the struck FOWT.

When both the striking ship and the struck FOWT are coupled using ALE, the peak contact force and deformation energy of the FOWT are significantly higher compared to MCOL simulations. The difference observed between MCOL and LS-DYNA/ALE is greater for an impact velocity of 2 m/s than for an impact velocity of 5 m/s.

Incorporating FSI coupling for the striking vessel demonstrated that the rigid body motions of both the striking ship and the struck FOWT are influenced by the bow waves generated by the approaching ship prior to collision. However, certain non-physical phenomena were observed when the striking ship was coupled with the surrounding water using the ALE method. Consequently, at present, the CEL approach implemented in LS-DYNA/ALE cannot be reliably employed as a benchmark tool to validate studies on ship collisions with FOWTs. This methodology requires further investigation to better model the interaction between the striking ship and the surrounding water.

7.1 Challenges in the CEL Approach

In addition to the limitations of the ALE and penalty coupling algorithm (section-3.1.3), modelling the collision event using LS-DYNA/ALE presented several additional challenges. The buoyancy forces could not be correctly modelled in LS-DYNA/ALE. This created a need to impose artificial constraints on the heave DOFs. As a result, the physics of the collision event modelled using the CEL approach changed. By changing the boundary conditions applied on the heave DOF of the striking ship and the struck FOWT, the results of the peak contact force and deformation changed.

Another major drawback associated with the penalty coupling algorithm concerns the choice of coupling parameters. As discussed in section 5.2, the FSI forces in LS-DYNA/ALE are highly sensitive to the value of PFAC. The ALE method in LS-DYNA was developed primarily to simulate problems of short duration, such as bird impacts, slamming or wave impacts. The existing guidelines for modeling FSI using LS-DYNA/ALE (LS-DYNA Aerospace Working Group 2022) focus on preventing fluid leakage through the fluid-structure interface. This approach works well for simulating events such as slamming (Yu et al. 2019). However, the efficacy of this approach in accurately representing FSI forces in ship collisions remains uncertain.

Currently, no specific guidelines exist for modeling FSI of large floating bodies using LS-DYNA/ALE. The appropriate choice of coupling parameters can only be determined through trial and error. Consequently, a significant amount of computational time is required to identify the coupling parameters that can accurately represent FSI forces during ship collisions. The choice of coupling parameters, particularly the coupling stiffness is also specific to the mesh and the event being simulated. Each simulation requires its own calibration with respect to the coupling stiffness. The mesh size, critical time-step and the coupling stiffness are closely related to each other. Hence, the results obtained from LS-DYNA/ALE cannot be generalized based on the same coupling parameters. This restricts the use of LS-DYNA/ALE as a benchmark tool to validate other numerical methods.

7.2 Computation Efforts

All LS-DYNA/MCOL simulations were performed using LS-DYNA version : SMP d R11.0.0 (revision : 129956) whereas all CEL simulations were performed using LS-DYNA version: MPP d R14 (revision: R14.0-515-g8a12796b62) with 128 cores. Moreover, the end times for the CEL are higher than that of LS-DYNA/MCOL, because in CEL simulations, additional time is needed to impose gravity loads and allow for the ship travel before impact. Hence, a direct comparison of the computational times cannot be made. A more convenient and meaningful way to compare the computational efforts, is to compare the ratio of CPU time to the total simulation end-times for each simulation.

From table-6, it can be seen that even with the use of MPP, the CPU times (measured as a ratio of total simulation end time) required by the CEL simulations are approximately eight times

Table 6: Comparison of simulation times for MCOL and S-ALE

Simulation End Time	MCOL		S-ALE	
	7.5 seconds		12 seconds	
	Time [s]	**Ratio**	**Time [s]**	**Ratio**
MPP Decomposition	-	-	1.2945×10^{1}	1.079
Shell Element Processing	4.1400×10^{2}	55.200	4.2938×10^{1}	3.578
Solid Element Processing	-	-	1.4457×10^{3}	120.475
Contact Algorithm	1.9000×10^{2}	25.333	1.1508×10^{3}	95.900
S-ALE FSI	-	-	4.9898×10^{3}	415.817
S-ALE Advection	-	-	1.0875×10^{4}	906.250
Total CPU Time	2.3150×10^{3}	308.667	2.8426×10^{4}	2368.833

higher than MCOL simulations. The advection phase and penalty coupling for S-ALE are the highest contributors to this increased computational effort. The S-ALE simulation compared in table-6 had 445320 solid elements representing the fluid domain.

7.3 Scope for Future Work

Improvements in CEL simulations

The results from the current research indicate that modelling FSI for ship collisions using LS-DYNA/ALE, lack proper guidelines. A stable floating equilibrium position could not be achieved for the FOWT using the modelling methods described in chapter - 4. Using different approaches for representing the fluids (Material and Equation-of-state models), and the semi-infinite domain could possibly help in improving FSI modelling and eliminate the need to impose artificial constraints on the ship and FOWT. Similarly, setting up a well-defined procedure to identify the correct coupling parameters is essential to continue using LS-DYNA/ALE for further studies related to ship collisions with FOWTs.
As observed in section-6.3.5, modelling FSI of the striking ship using LS-DYNA/ALE produced non-physical results. The real cause of this behavior could not be determined. This problem could be further investigated. One possibility is to increase the extents of the fluid domain and study its effects.

Improvements to MCOL solver

From the results shown in section-6.3, it is evident that the ship wave can have an influence on the dynamics of collision. A similar observation was also made by Song et al. (2016). The current MCOL solver cannot capture the effect of bow and stern wave. Development of analytical or semi-empirical formulations to represent the effect of bow and stern waves in MCOL can help in better modelling the dynamics of ship collisions. Since the results obtained from LS-DYNA/ALE, regarding the bow and stern wave effects are not trustworthy, other numerical or experimental methods are needed to validate these effects of the bow and stern wave.

Detailed Modelling & Parametric Studies

In the current study, a reference OSV of 3190 tons was used as the striking ship and was modelled as a completely rigid body. To make the simulations more realistic, the bow of the striking ship can also be modelled as a deformable body. It can also be seen from figure-24 that the deformation energy can continue to increase even after loss of contact. The cross-section and mass distribution of the modelled FOWT tower will influence the global bending and such increase of deformation energy after contact. Hence, to better model these effects, the stiffening system of the FOWT must also be modelled. The current thesis work focused on analyzing the structural damage to FOWTs subjected to ship collisions. The components of RNA maybe damaged by high accelerations (Zhang et al. 2021). It is advisable to also observe the accelerations of the RNA for future parametric studies of ship-FOWT collisions.

Several other parametric studies can be performed to analyze the effect of bow rake angle & OSV hull forms. Most recent OSVs are designed with inverted bows or vertical bows. For such hull forms, a higher influence of the bow wave can be expected on the motion of the FOWT. Verification of these results requires either accurate modeling approaches in CEL simulations or the application of well-established, validated numerical methods such as BEM solvers or computational fluid dynamics based on Reynolds Averaged Navier-Stokes Equation (RANSE). Such verification is essential to ensure the reliability and accuracy of the simulated FSI forces during ship collision events.

Acknowledgement

I would like to express my sincere gratitude to my supervisor Hervé Le Sourne, ICAM for his unwavering trust, guidance, and care throughout this thesis journey. I am deeply indebted to Ye Pyae Sone Oo from ICAM for his extended support, particularly regarding the use of LS-DYNA. Their expertise and patience have significantly contributed to my learning experience and the quality of this thesis. Their support has been instrumental in shaping both my work and my understanding of the research process. This thesis has not only enhanced my conceptual understanding but has also provided me with valuable insights into the nature of research and the critical evaluation of research outcomes. For this enriching experience, I am truly grateful.

My heartfelt thanks go to Professor Lionel Gentaz from École Centrale de Nantes, for his invaluable assistance with all resistance calculations using REVA. His contributions have been crucial to the success of this research. I would also like to acknowledge Ian Do from Ansys for his prompt and helpful replies on LS-DYNA learning forums, which helped verify my understanding of the methods used in this study.

My gratitude extends to all professors and administrative staff of the EMSHIP+ program. A special mention goes to professor Philippe Rigo, the coordinator of the EMSHIP+ program, whose support has been pivotal in my successful completion of this course. I would also like to extend my sincere thanks to all my school teachers who laid the foundation of my education, and to the professors from my bachelor's degree program who nurtured my passion for engineering and prepared me for advanced studies.

Lastly, I would like to thank my family and friends for their constant motivation and support through all the challenges I have faced. Your encouragement has been my strength throughout this journey.

REFERENCES

Aquelet, Nicolas and Mhamed Souli (2013). "ALE Incompressible Fluid in LS-DYNA". In: *9th European LS-DYNA Conference*. URL: *https://www.dynalook.com/conferences/9th-european-ls-dyna-conference/ale-incompressible-fluid-in-ls-dyna*.

Bela, Andreea, Hervé Le Sourne, Loïc Buldgen, and Philippe Rigo (2017). "Ship collision analysis on offshore wind turbine monopile foundations". In: *Marine Structures* 51, pp. 220–241. ISSN: 0951-8339. DOI: *https://doi.org/10.1016/j.marstruc.2016.10.009*. URL: *https://www.sciencedirect.com/science/article/pii/S0951833916302519*.

Buitendijk, Mariska (Feb. 2022). *Julietta D damages wind turbine foundation, master and chief officer under suspicion*. URL: *https://swzmaritime.nl/news/2022/02/03/julietta-d-damages-wind-turbine-foundation-master-and-chief-officer-under-suspicion/* (visited on 05/24/2024).

Buljan, Adrijana (May 2023). *Cargo Ship-Hit Gode Wind 1 Turbine Went Back Into Service in 24 Hours; Vessel Said to Have Been Kilometres Off Course*. URL: *https://www.offshorewind.biz/2023/05/30/cargo-ship-hit-gode-wind-turbine-went-back-into-service-in-24-hours-vessel-said-to-have-been-kilometres-off-course/* (visited on 05/24/2024).

Chaaban, Rannam and C.P. Fritzen (2014). "Reducing Blade Fatigue and Damping Platform Motions of Floating Wind Turbines Using Model Predictive Control". In: URL: *https://api.semanticscholar.org/CorpusID:164211842* (visited on 07/17/2024).

Chen, Hao (2020). "The New S-ALE FSI Solver". In: *16th European LS-DYNA Conference*. URL: *https://lsdyna.ansys.com/wp-content/uploads/attachments/t8-1-b-fsi-ale-081.pdf*.

ClassNK (2023). *Research and Development on Ship Collisions*. URL: *https://www.classnk.or.jp/hp/pdf/research/rd/2023/08_e08.pdf* (visited on 06/30/2024).

Donea, Jean, Antonio Huerta, J.-Ph. Ponthot, and A. Rodríguez-Ferran (Aug. 2004). "Arbitrary Lagrangian–Eulerian Methods". In: Wiley. DOI: *10.1002/0470091355.ecm009*.

LS-DYNA Aerospace Working Group (June 2022). *LS-DYNA Aerospace Working Group Modeling Guidelines Document*. Version 22-1. URL: *https://awg.ansys.com/tiki-download_file.php?fileId=2173*.

Echeverry Jaramillo, Sara (2021). "Numerical and analytical study of a spar-like floating offshore wind turbine impacted by a ship". Doctoral Dissertation. University of Liegé.

Echeverry Jaramillo, Sara, Lucas Márquez, Philippe Rigo, and Hervé Le Sourne (2019). "Numerical crashworthiness analysis of a spar floating offshore wind turbine impacted by a ship". In: *Developments in the Collision and Grounding of Ships and Offshore Structures*. URL: *https://api.semanticscholar.org/CorpusID:216222922*.

FERRY, Michel (2002a). *MCOL - Theoretical Manual*. Technical Report. Nantes, France: Principia Marine.

— (2002b). *MCOL- User's Manual*. Technical Report. Nantes, France: Principia Marine.

Förster, Christiane, Wolfgang A. Wall, and Ekkehard Ramm (Jan. 2007). "Artificial added mass instabilities in sequential staggered coupling of nonlinear structures and incompressible viscous flows". In: *Computer Methods in Applied Mechanics and Engineering* 196 (7), pp. 1278–1293. ISSN: 00457825. DOI: *10.1016/j.cma.2006.09.002*.

Gagnon, R.E. and A. Derradji-Aouat (2006). "First Results of Numerical Simulations of Bergy Bit Collisions with the CCGS Terry Fox Icebreaker". In: *Proceedings of IAHR 2006*. Sapporo, Japan.

Gagnon, R.E. and J. Wang (2012). "Numerical simulations of a tanker collision with a bergy bit incorporating hydrodynamics, a validated ice model and damage to the vessel". In: *Cold Regions Science and Technology* 81, pp. 26–35. ISSN: 0165-232X. DOI: *https://doi.org/10.1016/j.coldregions.2012.04.006*. URL: *https://www.sciencedirect.com/science/article/pii/S0165232X12000870*.

Guo, Jiamin, Yu Zhao, Weigang Chen, and Guangeng Zhou (2022). "Simulation of a Ship and Tension Leg Platform Wind Turbine Collision". In: *Journal of Marine Science and Technology* 29.6, Article 2. DOI: *10.51400/2709-6998.2553*. URL: *https://jmstt.ntou.edu.tw/journal/vol29/iss6/2*.

Hilburger, Mark W. (Dec. 2020). *Buckling of Thin-Walled Circular Cylinders*. NASA Special Publication NASA/SP-8007-2020/REV 2. Hampton, VA: NASA. URL: *https://shellbuckling.com/papers/classicNASAReports/NASA-SP-8007-2020Rev2FINAL.pdf*.

Ian, Do and Day Jim (2005). *An Overview of the Arbitrary Lagrangian-Eulerian (ALE) Capability in LS-DYNA*. Online PDF. Accessed: 2024-03-12. Livermore Software Technology Corporation. URL: *https://ftp.lstc.com/anonymous/outgoing/support/FAQ_docs/ale_overview_short2.pdf*.

Jonkman, J., S. Butterfield, W. Musial, and G. Scott (2009). *Definition of a 5-MW reference wind turbine for offshore system development*. Tech. rep. NREL/TP-500-38060. National Renewable Energy Lab.(NREL), Golden, CO (United States).

Jonkman, Jason (2010). *Definition of the Floating System for Phase IV of OC3*. NREL Technical Report NREL/TP-500-47535. Golden, Colorado: National Renewable Energy Laboratory (NREL). URL: *https://www.nrel.gov/docs/fy10osti/47535.pdf*.

Ladeira, M., H. Le Sourne, P. Echeverry, and P. Rigo (2023). "Assessment of the Energy Balance Gap in Ship-FOWT Collision Simulations with LS-DYNA and MCOL". In: *Proceedings of the 9th International Conference on Marine Structures*. Ed. by C. Guedes Soares and A.P. Teixeira. CRC Press. DOI: *10.1201/9781003230373-26*.

Le Sourne, Hervé, Nicolas Couty, Fermín Besnier, Cyrille Kammerer, Hervé Legavre, and Principia Marine (Jan. 2003). "LS-DYNA Applications in Shipbuilding". In.

Le Sourne, Hervé, E.R. Donner, Fermín Besnier, and Michel Ferry (June 2001). "External dynamics of ship-submarine collision". In.

LS-DYNA Keyword User's Manual (2024a). R15. Livermore Software Technology Corporation. URL: *https://ftp.lstc.com/anonymous/outgoing/web/ls-dyna_manuals/R15/LS-DYNA_Manual_Volume_I_R15.pdf*.

LS-DYNA Keyword User's Manual (2024b). R15. Livermore Software Technology Corporation. URL: *https://ftp.lstc.com/anonymous/outgoing/web/ls-dyna_manuals/R15/LS-DYNA_Manual_Volume_II_R15.pdf*.

LS-DYNA Theory Manual (Feb. 2024). R15. Livermore Software Technology Corporation. Livermore, California. URL: *https://ftp.lstc.com/anonymous/outgoing/web/ls-dyna_manuals/R15/LS-DYNA_Manual_Theory_R15.pdf*.

Meicke, Stephen A. (Aug. 2011). *Title: Hydroelastic Modeling of a Wave Energy Converter Using the Arbitrary Lagrangian-Eulerian Finite Element Method in LS-DYNA*. URL: *https://ir.library.oregonstate.edu/downloads/9p290c593*.

Morison, J.R., J.W. Johnson, and S.A. Schaaf (May 1950). "The Force Exerted by Surface Waves on Piles". In: *Journal of Petroleum Technology* 2 (05), pp. 149–154. ISSN: 0149-2136. DOI: *10.2118/950149-G*.

Olovsson, Lars (Sept. 2006). *LS-DYNA Training class in ALE and fluid-structure interaction*. Livermore Software Technology Corporation. URL: *https://ftp.lstc.com/anonymous/outgoing/support/FAQ_docs/ALE_training_by_Lars.Sept06.pdf* (visited on 05/23/2024).

Petersen, Martin J. and Preben T. Pedersen (Apr. 1981). "Collisions Between Ships and Offshore Platforms". In: *Offshore Technology Conference*. Offshore Technology Conference. DOI: *10.4043/4134-MS*.

Safety4Sea (Apr. 2020). *Three crew injured in wind turbine allision off Germany*. URL: *https://safety4sea.com/three-crew-injured-in-wind-turbine-allision-off-germany/* (visited on 05/24/2024).

Song, Ming, Ekaternia Kim, Jørgen Amdahl, Jun Ma, and Yi Huang (2016). "A comparative analysis of the fluid-structure interaction method and the constant added mass method for ice-structure collisions". In: *Marine Structures* 49, pp. 58–75. ISSN: 0951-8339. DOI: *https://doi.org/10.1016/j.marstruc.2016.05.005*.

Song, Ming, Jun Ma, and Yi Huang (2017). "Fluid-structure interaction analysis of ship-ship collisions". In: *Marine Structures* 55, pp. 121–136. ISSN: 0951-8339. DOI: *https://doi.org/10.1016/j.marstruc.2017.05.006*. URL: *https://www.sciencedirect.com/science/article/pii/S0951833916301332*.

Stenius, Ivan and Anders Ros'en (2007). "FE-modelling of hydrodynamic hull-water impact loads". In: *6th European LS-DYNA Conference*. URL: *https://www.dynalook.com/conferences/european-conf-2007/fe-modelling-of-hydrodynamic-hull-water-impact.pdf/view*.

Storheim, Martin and Jørgen Amdahl (July 2014). "Design of offshore structures against accidental ship collisions". In: *Marine Structures* 37, pp. 135–172. ISSN: 09518339. DOI: *10.1016/j.marstruc.2014.03.002*.

Thavornpattanapong, Pongpat, Kelvin Wong, Sherman Cheung, and Jiyuan Tu (Jan. 2011). "Mathematical Analysis of Added-Mass Instability in Fluid-Structure Interaction". In: *International Journal of Applied Mathematics and Statistics* 10, pp. 43–51.

Vandegar, Gabriel (Aug. 2023). "Validation of the ColFOWT collision assessment tool for ship/offshore wind turbines". In: URL: *https://lib.uliege.behttps://matheo.uliege.be*.

Ye, Xudong, Wei Fan, Yanyan Sha, Xugang Hua, Qinglin Wu, and Yongli Ren (2023). "Fluid-structure interaction analysis of oblique ship-bridge collisions". In: *Engineering Structures* 274, p. 115129. ISSN: 0141-0296. DOI: *https://doi.org/10.1016/j.engstruct.2022.115129*. URL: *https://www.sciencedirect.com/science/article/pii/S0141029622012056*.

Yu, Zhaolong and Jørgen Amdahl (Apr. 2018). "A review of structural responses and design of offshore tubular structures subjected to ship impacts". In: *Ocean Engineering* 154, pp. 177–203. ISSN: 00298018. DOI: *10.1016/j.oceaneng.2018.02.009*.

Yu, Zhaolong, Jørgen Amdahl, Marilena Greco, and Huili Xu (May 2019). "Hydro-plastic response of beams and stiffened panels subjected to extreme water slamming at small impact angles, part II: Numerical verification and analysis". In: *Marine Structures* 65, pp. 114–133. ISSN: 09518339. DOI: *10.1016/j.marstruc.2019.01.003*.

Zhang, Yichi, Zhiqiang Hu, Chong Ng, Chunjiang Jia, and Zhe Jiang (Jan. 2021). "Dynamic responses analysis of a 5 MW spar-type floating wind turbine under accidental ship-impact scenario". In: *Marine Structures* 75, p. 102885. ISSN: 09518339. DOI: *10.1016/j.marstruc.2020.102885*.

Zong, Rui (2012). "Finite element analysis of ship-ice collision using LS-DYNA". Master's thesis. Memorial University of Newfoundland. URL: *http://research.library.mun.ca/2419/*.

APPENDIX A: FINITE ELEMENT MODEL OF FOWT

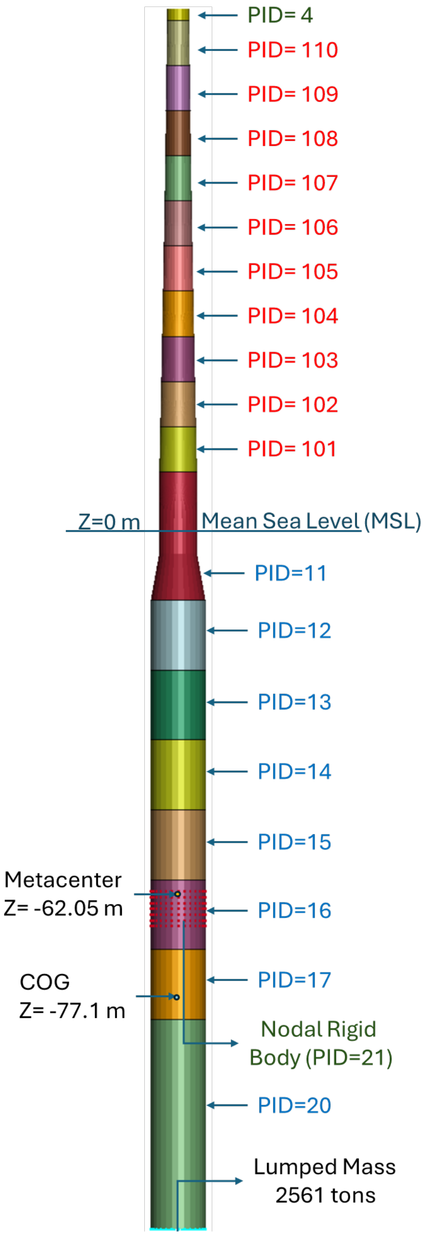

PID	Z_{bottom} $[m]$	Z_{top} $[m]$	$N_{elements}$	t $[mm]$	t_{cr} $[mm]$	ρ $[kg/m^3]$	Mass $[kg]$
4	87.60	89.60	124	22	-	7800	350000.00
110	79.84	87.60	288	19.8	-	8200	15550.44
109	72.08	79.84	312	20.6	-	8200	16888.10
108	64.32	72.08	312	21.4	-	8200	18408.17
107	56.56	64.32	312	22.2	-	8200	20119.11
106	48.80	56.56	340	23	-	8200	22021.67
105	41.04	48.80	364	23.8	-	8200	24109.31
104	33.28	41.04	604	24.6	-	8200	26370.98
103	25.52	33.28	836	25.4	-	8200	28816.84
102	**17.76**	**25.52**	**2232**	**26.2**	**-**	**8200**	**31410.79**
101	**10.00**	**17.76**	**3900**	**27**	**-**	**8200**	**34174.53**
11	**-12.00**	**10.00**	**2376**	**90**	**80.07**	**7800**	**342589.46**
12	-24.00	-12.00	336	100	92.54	7800	275829.98
13	-36.00	-24.00	336	110	102.33	7800	303412.36
14	-48.00	-36.00	336	120	110.54	7800	330994.64
15	-60.00	-48.00	336	130	117.68	7800	358577.53
16	-72.00	-60.00	336	150	124.05	7800	413743.30
17	-84.00	-72.00	336	250	129.82	7800	689572.17
20	-120.00	-84.00	1140	250	144.63	7800	4764155.10
Total No of Shell Elements			**15156**				

$$p_{cr} = \frac{\gamma E}{4(1-\nu^2)} \left(\frac{t}{r}\right)^3 \tag{8}$$

The critical thickness to avoid buckling (t_{cr}) is calculated using equation - 8. The value of γ is taken as 0.8. Young's Modulus (E) = 210 GPa and Poisson's ratio (ν) = 0.33.

Due to nature of penalty coupling, the actual external pressure might be higher than the expected hydrostatic pressure. Hence, the value of p_{cr} for equation - 8 is calculated as $1.05 \times (101325 + \rho \cdot g \cdot H_{max})$.

The parts highlighted in bold (PID = 11,101,102) are grouped into a part set and, defined as slave parts for contact with the ship bow.

The mass of PID 20 shown in the table, includes the lumped mass added to the bottom face.

APPENDIX B: KEYWORDS USED FOR CEL SIMULATIONS

Modelling the Fluid Domain

```
$# LS-DYNA Keyword file created by LS-PrePost(R) 2024/R1(4.11.2)-27Mar2024
$# Created on Jul-8-2024 (15:38:09)
*KEYWORD
*TITLE
$======================================================================================
$ S-ALE mesh definition
$ Use high numbers for nbid and ebid to avoid overlap with lagrangian parts
$======================================================================================
*ALE_STRUCTURED_MESH
$#   mshid      dpid      nbid      ebid    unused    unused    unused    tdeath
         2         2    700001    700001                              1.00000E16
$#   cpidx     cpidy     cpidz      nid0     lcsid
      2001      2002      2003         0         0
*ALE_STRUCTURED_MESH_CONTROL_POINTS
$#    cpid    unused     icase       sfo    unused      offo
      2001                   0       1.0                 0.0
$#                  n                   x            ratio/xl
                    1              -130.0                 0.0
                  113               -18.0                 0.0
                  171                40.0                 0.0
*ALE_STRUCTURED_MESH_CONTROL_POINTS
$#    cpid    unused     icase       sfo    unused      offo
      2002                   0       1.0                 0.0
$#                  n                   x            ratio/xl
                    1               -18.0                 0.0
                   37                18.0                 0.0
*ALE_STRUCTURED_MESH_CONTROL_POINTS
$#    cpid    unused     icase       sfo    unused      offo
      2003                   0       1.0                 0.0
$#                  n                   x            ratio/xl
                    1              -160.0                 0.0
                  141               -20.0                 0.0
                  161                 0.0                 0.0
                  166                 5.0                 0.0
$======================================================================================
$ Define a box and trim unwanted S-ALE elements below ship domain
$======================================================================================
*DEFINE_BOX_TITLE
Trim SALE Mesh
$#   boxid       xmn       xmx       ymn       ymx       zmn       zmx
         2    -152.0     -18.0     -18.0      18.0    -160.0     -20.0
*ALE_STRUCTURED_MESH_TRIM
$#   mshid    option      oper    out/in     boxid        e2        e3        e4
         2BOXCOR             0         1         2       0.0       0.0       0.0
$======================================================================================
$======================================================================================
```

```
$ S-ALE mesh boundary conditions. Free slip but no normal movement of nodes in outer
$ faces. Since mesh trimming is used, the correct nodal points must be used to define
$ the outer faces.
$=====================================================================================
*BOUNDARY_SPC_SET_ID
$#      id                                                               heading
        21XFACE
$#    nsid       cid      dofx      dofy      dofz     dofrx     dofry     dofrz
        21         0         1         0         0         0         0         0
*SET_NODE_GENERAL_TITLE
XFACE
$#     sid       da1       da2       da3       da4    solver       its         -
        21       0.0       0.0       0.0       0.0MECH               1
$#  option     mshid      imin      imax      jmin      jmax      kmin      kmax
SALECPT            2       171       171         1        37         1       166
SALECPT            2         1         1         1        37       141       166
SALECPT            2       113       113         1        37         1       141
$-------------------------------------------------------------------------------------
*BOUNDARY_SPC_SET_ID
$#      id                                                               heading
        22YFACE
$#    nsid       cid      dofx      dofy      dofz     dofrx     dofry     dofrz
        22         0         0         1         0         0         0         0
*SET_NODE_GENERAL_TITLE
YFACE
$#     sid       da1       da2       da3       da4    solver       its         -
        22       0.0       0.0       0.0       0.0MECH               1
$#  option     mshid      imin      imax      jmin      jmax      kmin      kmax
SALECPT            2         1       113         1         1       141       166
SALECPT            2         1       113        37        37       141       166
SALECPT            2       113       171         1         1         1       166
SALECPT            2       113       171        37        37         1       166
$-------------------------------------------------------------------------------------
*BOUNDARY_SPC_SET_ID
$#      id                                                               heading
        23ZFACE
$#    nsid       cid      dofx      dofy      dofz     dofrx     dofry     dofrz
        23         0         0         0         1         0         0         0
*SET_NODE_GENERAL_TITLE
ZFACE
$#     sid       da1       da2       da3       da4    solver       its         -
        23       0.0       0.0       0.0       0.0MECH               1
$#  option     mshid        -x        +x        -y        +y        -z        +z
SALEFAC            2         0         0         0         0         0         1
SALECPT            2         1       113         1        37       141       141
SALECPT            2       113       171         1        37         1         1
$=====================================================================================
$ Gravity loading
$ Acceleration due to gravity is modelled to act in +Z direction so gravitational
$ force acts in -Z
$=====================================================================================
*LOAD_BODY_Z
```

```
$#    lcid        sf    lciddr        xc        yc        zc       cid
         6   9.80665         0       0.0       0.0       0.0         0
$-------------------------------------------------------------------------------
$ A vector pointing in -Z direction is needed to specify direction of gravity for
$ hydrostatic cards.
$-------------------------------------------------------------------------------
*DEFINE_VECTOR_TITLE
Gravity
$#     vid        xt        yt        zt        xh        yh        zh       cid
         6      20.0      20.0       0.0      20.0      20.0      -1.0         0
$-------------------------------------------------------------------------------
$ Magninute of gravity loading is increased over a duration of 0.5 seconds.
$ This helps in reducing pressure fluctuations in the fluid domain
$-------------------------------------------------------------------------------
*DEFINE_CURVE_SMOOTH_TITLE
Gravity
$#    lcid      sidr      dist    tstart      tend     trise      vmax
         6         0     400.0       0.0       0.0       0.5       1.0
$===============================================================================
$ These nodes define the waterplane for filling the mesh. They must remain fixed.
$===============================================================================
*NODE
$#   nid               x               y               z      tc      rc
  600001             0.0             0.0             5.0       0       0
  600002             0.0             0.0             0.0       0       0
*BOUNDARY_SPC_NODE
$#     nid       cid      dofx      dofy      dofz     dofrx     dofry     dofrz
    600001         0         1         1         1         1         1         1
    600002         0         1         1         1         1         1         1
$===============================================================================
$ Fluid Materials and EQUATION OF STATE
$===============================================================================
*HOURGLASS_TITLE
hourglass
$#    hgid       ihq        qm       ibq        q1        q2    qb/vdc        qw
         1         21.00000E-6         0       1.5      0.06       0.1       0.1
$-------------------------------------------------------------------------------
*MAT_NULL_TITLE
WATER
$#     mid        ro        pc        mu     terod     cerod        ym        pr
        33    1025.0     -10.0   0.00179       0.0       0.0       0.0       0.0
*EOS_LINEAR_POLYNOMIAL_TITLE
WATER-LinearPoly
$#   eosid        c0        c1        c2        c3        c4        c5        c6
         3  101300.02.250000E9       0.0       0.0       0.0       0.0       0.0
$#      e0        v0
       0.0       1.0
$-------------------------------------------------------------------------------
*MAT_NULL_TITLE
AIR
$#     mid        ro        pc        mu     terod     cerod        ym        pr
        44      1.18     -10.01.18400E-5       0.0       0.0       0.0       0.0
```

```
*EOS_LINEAR_POLYNOMIAL_TITLE
AIR
$#   eosid        c0        c1        c2        c3        c4        c5        c6
         4       0.0       0.0       0.0       0.0       0.4       0.4       0.0
$#      e0        v0
  253300.0       1.0
$=====================================================================================
$ MULTI MATERIAL GROUPS AND FILLING THE S-ALE MESH
$ AMMGIDs are defined in order of appearance.
$ AMMGID 1 = Air Outside
$ AMMGID 2 = Water Outside
$ AMMGID 3 = Air Inside
$-------------------------------------------------------------------------------------
*ALE_STRUCTURED_MULTI-MATERIAL_GROUP
$#  ammgnm       mid     eosid    unused    unused    unused    unused      pref
         1        44         4                                          101325.0
$#  ammgnm       mid     eosid    unused    unused    unused    unused      pref
         2        33         3                                          101325.0
$#  ammgnm       mid     eosid    unused    unused    unused    unused      pref
         3        44         4                                          101325.0
$-------------------------------------------------------------------------------------
$ STEP 1 - Fill the complete mesh with water
$-------------------------------------------------------------------------------------
*ALE_STRUCTURED_MESH_VOLUME_FILLING
$#   mshid    unused    ammgto    unused   nsample    unused   unused-       vid
         2         2                             3                             0
$#    geom    in/out        e1        e2        e3        e4        e5
ALL               0       0.0       0.0       0.0       0.0       0.0
$-------------------------------------------------------------------------------------
$ STEP 2 - Fill above the waterplane with air
$-------------------------------------------------------------------------------------
*ALE_STRUCTURED_MESH_VOLUME_FILLING
$#   mshid    unused    ammgto    unused   nsample    unused   unused-       vid
         2         1                             3                             0
$#    geom    in/out      nid1      nid2        e3        e4        e5
PLANE             0    600002    600001         0         0         0
$-------------------------------------------------------------------------------------
$ STEP 3 - Fill Inside the part-set (Turbine & Ship) with air
$-------------------------------------------------------------------------------------
*ALE_STRUCTURED_MESH_VOLUME_FILLING
$#   mshid    unused    ammgto    unused   nsample    unused   unused-       vid
         2         3                             3                             0
$#    geom    in/out      psid        e2        e3        e4        e5
PARTSET           1       101      0.05         0         0         0
$=====================================================================================
$ Define Ambient Elements for initializing Hydrostatic Pressure
$=====================================================================================
*SET_SOLID_GENERAL_TITLE
Ambient Boundaries
$#     sid    solver
         2MECH
$#  option     mshid      imin      imax      jmin      jmax      kmin      kmax
```

```
SALECPT            2         1         3         1        37       141       161
SALECPT            2       169       171         1        37       141       161
SALECPT            2         3       113         1         3       141       161
SALECPT            2         3       113        35        37       141       161
SALECPT            2         3       115         3        35       141       143
SALECPT            2       113       171         1         3         1       161
SALECPT            2       113       171        35        37         1       161
SALECPT            2       113       171         3        35         1         3
SALECPT            2       113       115         3        35         1       143
SALECPT            2       169       171         3        35         1       143
SALECPT            2         1         3         1        37       161       166
SALECPT            2       169       171         1        37       161       166
SALECPT            2         3       169         1         3       161       166
SALECPT            2         3       169        35        37       161       166
$===============================================================================
*SET_SOLID_GENERAL_TITLE
AmbientWater
$#     sid    solver
        33MECH
$#  option     mshid      imin      imax      jmin      jmax      kmin      kmax
SALECPT            2         1         3         1        37       141       161
SALECPT            2       169       171         1        37       141       161
SALECPT            2         3       113         1         3       141       161
SALECPT            2         3       113        35        37       141       161
SALECPT            2         3       115         3        35       141       143
SALECPT            2       113       171         1         3         1       161
SALECPT            2       113       171        35        37         1       161
SALECPT            2       113       171         3        35         1         3
SALECPT            2       113       115         3        35         1       143
SALECPT            2       169       171         3        35         1       143
*SET_SOLID_GENERAL_TITLE
AmbientAir
$#     sid    solver
        44MECH
$#  option     mshid      imin      imax      jmin      jmax      kmin      kmax
SALECPT            2         1         3         1        37       161       166
SALECPT            2       169       171         1        37       161       166
SALECPT            2         3       169         1         3       161       166
SALECPT            2         3       169        35        37       161       166
$===============================================================================
$ By using same LCID for gravity loading, hydrostatic pressure in ambient domain is also
$ smoothly increased. No need of including *INITIAL_HYDROSTATIC_ALE
$===============================================================================
*ALE_AMBIENT_HYDROSTATIC
$#  alesid     stype     vecid      grav     pbase   ramptlc
         2         2         6   9.80665  101325.0         6
$#     nid     mmgbl
    600001         1
    600002         2
$===============================================================================
$ Multi-Material group sets are required to define FSI coupling cards.
$===============================================================================
```

```
*SET_MULTI_TITLE
Air Outside
$#  ammsid
        11
$# ammgid1   ammgid2   ammgid3   ammgid4   ammgid5   ammgid6   ammgid7   ammgid8
1         0         0         0         0         0         0         0
*SET_MULTI_TITLE
Water
$#  ammsid
        22
$# ammgid1   ammgid2   ammgid3   ammgid4   ammgid5   ammgid6   ammgid7   ammgid8
2         0         0         0         0         0         0         0
*SET_MULTI_TITLE
Air Inside
$#  ammsid
        33
$# ammgid1   ammgid2   ammgid3   ammgid4   ammgid5   ammgid6   ammgid7   ammgid8
3         0         0         0         0         0         0         0
$======================================================================================
*END
```

Listing 1: Fluid Domain Model

Simulation controls and boundary conditions

```
$# LS-DYNA Keyword file created by LS-PrePost(R) 2024/R1(4.11.2)-27Mar2024
$# Created on Jul-8-2024 (15:38:09)
*KEYWORD MEMORY=100M
$==================================================================================
*INCLUDE
SPAR_Def.k
SHIPDEF.k
Fluid.k
$==================================================================================
$ Control Cards
$==================================================================================
$*CONTROL_MPP_DECOMPOSITION_DISTRIBUTE_ALE_ELEMENTS
$----------------------------------------------------------------------------------
*CONTROL_ALE
$#     dct      nadv      meth      afac      bfac      cfac      dfac      efac
         0         1         3      -1.0       0.0       0.0       0.0       0.0
$#   start       end     aafac     vfact      prit       ebc      pref   nsidebc
       0.01.00000E20       1.01.00000E-6         1         0       0.0         0
$#    ncpl      nbkt    imascl    checkr    beamin   mmgpref    pdifmx   dtmufac
         1        50         0       0.1       0.0         0       0.0       0.0
$# optimpp    ialedr    bndflx    minmas
         0         0         01.00000E-5
$----------------------------------------------------------------------------------
*CONTROL_ENERGY
$#    hgen      rwen    slnten     rylen     irgen     maten     drlen     disen
         2         2         1         2         2         2         1         1
```

```
$-------------------------------------------------------------------------------
*CONTROL_HOURGLASS
$#     ihq        qh
         21.00000E-6
$-------------------------------------------------------------------------------
*CONTROL_TERMINATION
$#  endtim    endcyc     dtmin    endeng    endmas     nosol
      12.0         0       0.0       0.01.000000E8         0
$-------------------------------------------------------------------------------
*CONTROL_TIMESTEP
$#  dtinit    tssfac      isdo    tslimt     dt2ms      lctm     erode     ms1st
       0.0       0.0         0       0.0       0.0         0         0         0
$-------------------------------------------------------------------------------
*CONTROL_CONTACT
$#  slsfac    rwpnal    islchk    shlthk    penopt    thkchg     orien    enmass
       0.1       0.0         1         0         1         0         1         0
$#  usrstr    usrfrc     nsbcs    interm     xpene     ssthk      ecdt   tiedprj
         0         0         0         0       4.0         0         0         0
$#   sfric     dfric       edc       vfc        th     th_sf    pen_sf     ptscl
       0.0       0.0       0.0       0.0       0.0       0.0       0.0       1.0
$#  ignore    frceng   skiprwg    outseg   spotstp   spotdel   spothin   dir_tie
         0         0         0         0         0         0
$#    isym    nserod    rwgaps    rwgdth     rwksf      icov    swradf    ithoff
         0         0         1       0.0       1.0         0       0.0         0
$#  shledg    pstiff    ithcnt    tdcnof     ftall    unused    shltrw    igactc
         0         0         0         0         0                 0.0         0
$===============================================================================
$ Allows to measure the energy of each material lost in advection step
$===============================================================================
*DATABASE_ALE_MAT
$#   dtout    boxlow     boxup      dtxy
    0.0167         0         0    0.0167
$===============================================================================
$ For ALE simulation with coupling ship to water, remove initial velocity specified
$ in the *PART_INERTIA keyword
$ The boundary conditions and imposed ship velocity are specified below.
$ death times are specified to remove the imposed boundary conditions where necessary
$===============================================================================
*BOUNDARY_PRESCRIBED_MOTION_RIGID_ID
$#      id                                                               heading
         0Ship Velocity
$#     pid       dof       vad      lcid        sf       vid     death     birth
        99         1         0         1       5.0         0       5.7       0.0
$#      id                                                               heading
         2ShipSway
$#     pid       dof       vad      lcid        sf       vid     death     birth
        99         2         0         3       1.0         0       5.7       0.0
$#      id                                                               heading
         3Ship Heave
$#     pid       dof       vad      lcid        sf       vid     death     birth
        99         3         0         3       1.0         01.00000E28       0.0
$#      id                                                               heading
```

```
         4shiproll
$#     pid       dof       vad      lcid        sf       vid     death     birth
        99         5         0         3       1.0         01.00000E28       0.0
$#      id                                                             heading
         5shippitch
$#     pid       dof       vad      lcid        sf       vid     death     birth
        99         6         0         3       1.0         0       5.7       0.0
$#      id                                                             heading
         6ShipYAW
$#     pid       dof       vad      lcid        sf       vid     death     birth
        99         7         0         3       1.0         01.00000E28       0.0
$#      id                                                             heading
         0SPAR heave
$#     pid       dof       vad      lcid        sf       vid     death     birth
        21         3         0         3       1.0         01.00000E28       0.0
$===============================================================================
$===============================================================================
*DEFINE_CURVE_SMOOTH_TITLE
Ship Velocity
$#    lcid      sidr      dist    tstart      tend     trise      vmax
         1         0     400.0       0.8       0.0       2.0       1.0
*DEFINE_CURVE_TITLE
InitalDisplacementZero
$#    lcid      sidr       sfa       sfo      offa      offo    dattyp     lcint
         3         0       1.0       1.0       0.0       0.0         0         0
$#                a1                  o1
                 0.0                 0.0
               100.0                 0.0
$===============================================================================
$ Definition of contact between ship bow and FOWT
$ The FOWT parts which are impacted by the ship are grouped into a part set and
$ specified as slave parts for the contact.
$===============================================================================
*CONTACT_AUTOMATIC_SURFACE_TO_SURFACE_MPP_ID
$#     cid                                                                 title
         0Ship-Tower Collision
$#  ignore      bckt    lcbckt    ns2trk   inititr    parmax    unused    cparm8
         0       200         0         3         2    1.0005                   0
$#  unused   chksegs     pensf   grpable         -     igtol
&                  0       1.0         0                 0.0
$#   surfa     surfb  surfatyp  surfbtyp   saboxid   sbboxid      sapr      sbpr
        99         1         3         2                             0         0
$#      fs        fd        dc        vc       vdc    penchk        bt        dt
       0.3       0.3       0.0       0.0       0.0                 0.01.00000E20
$#    sfsa      sfsb      sast      sbst     sfsat     sfsbt       fsf       vsf
       1.0       1.0                           1.0       1.0       1.0       1.0
$===============================================================================
$ FSI Coupling Cards Definition - SPAR
$===============================================================================
*ALE_STRUCTURED_FSI_TITLE
$#  coupid                                                                 title
         1To Water
```

```
$# lstrsid    alesid  lstrstyp   alestyp         -         -         -     mcoup
         1         2         2         1                                     -22
$#    start       end      pfac      fric         -      flip
       0.01.00000E101.00000E-4       0.0                   0
$--------------------------------------------------------------------------------
*ALE_STRUCTURED_FSI_TITLE
$#   coupid                                                                title
         3To Inside Air
$# lstrsid    alesid  lstrstyp   alestyp         -         -         -     mcoup
         1         2         2         1                                     -33
$#    start       end      pfac      fric         -      flip
       0.01.00000E101.00000E-5       0.0                   1
$================================================================================
$ FSI Coupling Cards Definition - SHIP
$================================================================================
*ALE_STRUCTURED_FSI_TITLE
$#   coupid                                                                title
         2SHIP To Outside Water
$# lstrsid    alesid  lstrstyp   alestyp         -         -         -     mcoup
        99         2         1         1                                     -22
$#    start       end      pfac      fric         -      flip
       0.01.00000E105.00000E-8       0.0                   0
$--------------------------------------------------------------------------------
*ALE_STRUCTURED_FSI_TITLE
$#   coupid                                                                title
         3SHIP To Inside Air
$# lstrsid    alesid  lstrstyp   alestyp         -         -         -     mcoup
        99         2         1         1                                     -33
$#    start       end      pfac      fric         -      flip
       0.01.00000E101.00000E-5       0.0                   1
$================================================================================
*END
```

Listing 2: Defining Controls, Contacts and Boundary Conditions

APPENDIX C: .MCO FILES USED FOR SHIP AND SPAR

SPAR

```
002$rigid body mass matrix (Mrb)
 0.8066E+07 0.0000E+00 0.0000E+00 0.0000E+00 0.0000E+00 0.0000E+00
 0.0000E+00 0.8066E+07 0.0000E+00 0.0000E+00 0.0000E+00 0.0000E+00
 0.0000E+00 0.0000E+00 0.8066E+07 0.0000E+00 0.0000E+00 0.0000E+00
 0.0000E+00 0.0000E+00 0.0000E+00 0.3395E+11-0.3698E+01 0.2735E-06
 0.0000E+00 0.0000E+00 0.0000E+00-0.3698E+01 0.3406E+11-0.2220E-06
 0.0000E+00 0.0000E+00 0.0000E+00 0.2735E-06-0.2220E-06 0.1405E+09
003$hydrostatic restoring matrix (Ks)
 0.0000E+00 0.0000E+00 0.0000E+00 0.0000E+00 0.0000E+00 0.0000E+00
 0.0000E+00 0.0000E+00 0.0000E+00 0.0000E+00 0.0000E+00 0.0000E+00
 0.0000E+00 0.0000E+00 3.3366E+05 0.0000E+00 0.0000E+00 0.0000E+00
 0.0000E+00 0.0000E+00 0.0000E+00 8.8108E+05 0.0000E+00 0.0000E+00
 0.0000E+00 0.0000E+00 0.0000E+00 0.0000E+00 8.8108E+05 0.0000E+00
 0.0000E+00 0.0000E+00 0.0000E+00 0.0000E+00 0.0000E+00 0.0000E+00
004$buoyancy parameters (xb,yb,zb,W=m*g,B=rho*g*displ,ZGref,PHIref,TETAref)
 0.0000E+00 0.0000E+00-1.5715E+01 7.9100E+07 7.9100E+07 0.0000E+00 0.0000E+00 0.0000E+00
005$added mass matrix (Ma)
 0.7893E+07 0.0000E+00 0.0000E+00 0.0000E+00 0.1226E+09 0.0000E+00
 0.0000E+00 0.7893E+07 0.0000E+00-0.1225E+09 0.0000E+00 0.0000E+00
 0.0000E+00 0.0000E+00 0.2381E+06 0.0000E+00 0.0000E+00 0.0000E+00
 0.0000E+00-0.1225E+09 0.0000E+00 0.9888E+10 0.0000E+00 0.0000E+00
 0.1226E+09 0.0000E+00 0.0000E+00 0.0000E+00 0.9890E+10 0.0000E+00
 0.0000E+00 0.0000E+00 0.0000E+00 0.0000E+00 0.0000E+00 0.5366E+04
006$nbsurf and viscous damping surfaces (rho,dCl/dalpa,Cd,A,nx,ny,nz,xc,yc,zc)
001
 0.1025E+04 0.0000E+00 0.6000E+00 1.1048E+03 0.0000E+00 0.1000E+01 0.0000E+00 0.0000E+00
     0.0000E+00 0.0000E+00
007$parameter for checking convergence (gosa0,accl)
 0.1000E-03 0.1000E+01
```

Listing 3: .mco file for SPAR

Ship

```
002$rigid body mass matrix (Mrb)
 0.3191E+07 0.0000E+00 0.0000E+00 0.0000E+00 0.0000E+00 0.0000E+00
 0.0000E+00 0.3191E+07 0.0000E+00 0.0000E+00 0.0000E+00 0.0000E+00
 0.0000E+00 0.0000E+00 0.3191E+07 0.0000E+00 0.0000E+00 0.0000E+00
 0.0000E+00 0.0000E+00 0.0000E+00 0.3901E+08 0.0000E+00 0.0000E+00
 0.0000E+00 0.0000E+00 0.0000E+00 0.0000E+00 0.1840E+11 0.0000E+00
 0.0000E+00 0.0000E+00 0.0000E+00 0.0000E+00 0.0000E+00 0.1836E+11
003$hydrostatic restoring matrix (K)
 0.0000E+00 0.0000E+00 0.0000E+00 0.0000E+00 0.0000E+00 0.0000E+00
 0.0000E+00 0.0000E+00 0.0000E+00 0.0000E+00 0.0000E+00 0.0000E+00
 0.0000E+00 0.0000E+00 9.3877E+06 0.0000E+00 0.0000E+00 0.0000E+00
 0.0000E+00 0.0000E+00 0.0000E+00 0.1630E+08 0.0000E+00 0.0000E+00
 0.0000E+00 0.0000E+00 0.0000E+00 0.0000E+00 0.3109E+09 0.0000E+00
 0.0000E+00 0.0000E+00 0.0000E+00 0.0000E+00 0.0000E+00 0.0000E+00
004$buoyancy parameters (xb,yb,zb,W,B,ZoGref,PHIref,TETAref)
 0.0000E+00 0.0000E+00 0.2302E+01 0.3130E+08 0.3130E+08 0.0000E+00 0.0000E+00 0.0000E+00
005$added mass matrix (Ma)
 0.7597E+05 0.0000E+00 0.0000E+00 0.0000E+00 0.7352E+07 0.0000E+00
 0.0000E+00 0.8818E+06 0.0000E+00-0.2004E+07 0.0000E+00 0.0000E+00
 0.0000E+00 0.0000E+00 0.4854E+07 0.0000E+00 0.0000E+00 0.0000E+00
 0.0000E+00-0.2005E+07 0.0000E+00 0.1525E+08 0.0000E+00 0.0000E+00
 0.7352E+07 0.0000E+00 0.0000E+00 0.0000E+00 0.1265E+10 0.0000E+00
 0.0000E+00 0.0000E+00 0.0000E+00 0.0000E+00 0.0000E+00 0.2432E+09
006$nbsurf and viscous damping surfaces
000
007$parameter for checking convergence (gosa0,accl)
 0.1000E-03 0.1000E+01
```

Listing 4: .mco file for Ship